

University of Louisville

ThinkIR: The University of Louisville's Institutional Repository

Electronic Theses and Dissertations

12-2022

Nonlinear observers for burning zone temperatures and torque estimation of the rotary cement kiln.

Bhagyashri Aditya Bhagwat
University of Louisville

Follow this and additional works at: <https://ir.library.louisville.edu/etd>



Part of the [Controls and Control Theory Commons](#)

Recommended Citation

Bhagwat, Bhagyashri Aditya, "Nonlinear observers for burning zone temperatures and torque estimation of the rotary cement kiln." (2022). *Electronic Theses and Dissertations*. Paper 3991.
Retrieved from <https://ir.library.louisville.edu/etd/3991>

This Doctoral Dissertation is brought to you for free and open access by ThinkIR: The University of Louisville's Institutional Repository. It has been accepted for inclusion in Electronic Theses and Dissertations by an authorized administrator of ThinkIR: The University of Louisville's Institutional Repository. This title appears here courtesy of the author, who has retained all other copyrights. For more information, please contact thinkir@louisville.edu.

NONLINEAR OBSERVERS FOR BURNING ZONE TEMPERATURE AND
TORQUE ESTIMATION OF THE ROTARY CEMENT KILN

By

Bhagyashri Aditya Bhagwat
B.E., Shivaji University, India, 2011
M.E., Shivaji University, India, 2014

A Dissertation
Submitted to the Faculty of the
J.B. Speed School of Engineering of the University of Louisville
in Partial Fulfillment of the Requirements
for the Degree of

Doctor of Philosophy
in Electrical Engineering

Department of Electrical and Computer Engineering
University of Louisville
Louisville, Kentucky

December 2022

NONLINEAR OBSERVERS FOR BURNING ZONE TEMPERATURE AND
TORQUE ESTIMATION OF THE ROTARY CEMENT KILN

By

Bhagyashri Aditya Bhagwat
B.E., Shivaji University, India, 2011
M.E., Shivaji University, India, 2014

A Dissertation approved on

August 4, 2022

by the following Dissertation Committee:

Michael L. McIntyre, Dissertation Director

Tamer Inanc

William Mark McGinley

John F. Naber

ABSTRACT

CONTROL AND OBSERVATION OF ROTARY CEMENT KILN

Bhagyashri Bhagwat

August 4, 2022

Due to consistent expansion in the infrastructure and housing sectors worldwide have given a new way for the rapid growth of global cement market. Increased global demand for the cement production makes the attractive research topic which can lead to the quality and overall efficiency of the product. Measurement of the temperature in the burning zone is vital to maintain product quality and kiln efficiency in the cement industry. Often the BZT is un-measurable due to internal kiln conditions, dusty environment, extreme heat, harshness for example and this leads to kiln not being driven as efficient as possible. Multi-physics tools are core to modern engineering, and smart manufacturing, but have not been extensively utilized in this low-cost industry, hence proposed approach is to find a reduced ordered model (ROM) of the thermodynamics of the kiln using data centric approach along with Multiphysics tool.

TABLE OF CONTENTS

ABSTRACT.....	iii
LIST OF FIGURES	vii
1 INTRODUCTION.....	1
1.1 CEMENT PROCESS BACKGROUND.....	2
1.2 CURRENT CONTROL/OBSERVATION STRATEGIES FOR ROTARY KILN	4
1.3 MOTIVATION FOR RESEARCH	6
1.4 OBJECTIVES.....	7
2. EXPERIMENTAL PLATFORM.....	10
2.1. PYROMETER LABVIEW INTERFACE.....	11
2.2 THERMOCOUPLE - LABJACK INTERFACE.....	11
2.3 MASS FLOW CONTROLLER.....	12
2.4 LAB SCALE KILN TEST RESULTS	13
3 REDUCED OREDR THERMAL MODEL APPROACH	17
3.1 THERMAL PARAMETER ESTIMATION.....	20
3.2 BURNING ZONE TEMPERATURE AND HEAT RATE OBSERVER DEVELOPMENT.....	24

3.2.1. ALUMINA TUBE TEMPERATURE OBSERVER DEVELOPMENT ($T_1(t)$)	24
3.2.2. HEAT RATE OBSERVER DEVELOPMENT.....	25
3.2.3 STABILITY ANALYSIS	27
3.3 EXPERIMENTAL RESULTS.....	29
3.3.1 THERMAL CIRCUIT PARAMETER ESTIMATION.....	29
3.3.2 OBSERVER DEVELOPMENT	30
4 ROTARY KILN SYSTEM MODEL	34
4.1 ROTARY KILN DYNAMIC SYSTEM MODEL	35
4.2 TORQUE OBSERVER DEVELOPMENT.....	36
4.2.1 OBSERVER DEVELOPMENT	36
4.2.2 STABILITY ANALYSIS	39
4.2.3 SIMULATION RESULTS.....	41
4.3 TORQUE OBSERVER VALIDATION RESULTS	44
5 CONTROL DEVELOPMENT	45
5.1 PERMANENT MAGNET DIRECT CURRENT MOTOR MODEL	45
5.1.1 PMDC MOTOR MODELING.....	45
5.1.2 PMDC CONTROLLER DEVELOPMENT	47
5.1.3 SPEED CONTROL TEST RESULTS.....	48
6. FUTURE WORK.....	50

CONCLUSION.....	52
CURRICULUM VITAE.....	56

LIST OF FIGURES

Figure 1: Global cement market size (2018-2029)	1
Figure 2: A production scale cement plant	2
Figure 3: Lab scale rotary kiln setup.....	10
Figure 4: Pyrometer-LabVIEW Interface	11
Figure 5: Labjack assembly inside the enclosure for temperature measurement	12
Figure 6: Mass flow controller connection with cRIO 9064	13
Figure 7: Test run results (09/22/2021)	14
Figure 8: Test run results (10/05/2021)	14
Figure 9: Test run results (10/08/2021)	14
Figure 10: Test run results (10/14/2021)	14
Figure 11: Test run results (12/07/2021)	15
Figure 12: Test run results (12/15/2021)	15
Figure 13: Pyrometer temperature profile.....	15
Figure 14: Temperature plot at the time material flowing through the kiln	16
Figure 15: Illustration for modeling kiln as slices	18
Figure 16: 2-D model and cross section of the kiln representing different layers and thermocouple position.....	18
Figure 17: Thermal resistance and capacitor network	19
Figure 18: Estimation results for parameter R_1 , C_1	29
Figure 19: Estimation results for parameter R_2 , C_2	30

Figure 20: Observed temperature vs validated temperature of the alumina tube for slice 1 without meal.....	32
Figure 21: Observed temperature vs validated temperature of the alumina tube for slice 1 with meal.....	32
Figure 22: Heat rate observer results for three slices.....	33
Figure 23: Kiln, burden and drive train	34
Figure 24: Schematic representation of the torque observer scheme for rotary kiln	37
Figure 25: Actual vs observed speed for rotary kiln.....	42
Figure 26: Speed observer error for rotary kiln	42
Figure 27: Actual torque vs observed torque for rotary kiln	42
Figure 28: Torque observer error for rotary kiln	43
Figure 29: Validated observed kiln torque with actual motor speed vs reference speed..	44
Figure 30: Motor control bench top testing system	46
Figure 31: Block diagram of PI controller for PMDC motor with modeling	47
Figure 32: PMDC Speed control drive – LabVIEW interface.....	48
Figure 33: Reference speed vs kiln speed.....	49
Figure 34: PI Controller output.....	49

1 INTRODUCTION

Concrete is the foundation of just about everything. Concrete is responsible for modern civilization, everyday walking sidewalks to aircraft runways, drinking water concrete pipes to concrete jungles, cities. In fact, it is so popular that it's the most widely used man-made product on earth. It is the highest consumed product on earth besides water. For every person in the world, about three tons of concrete gets used every year. It has been very durable, sustainable, resilient material for 1000s of years. Afterall it was essentially concrete that built Rome 1000s of years ago. To make concrete we need cement first.

The Cement Industry is one of the main industries considered as a backbone for sustainable development in the world. The consumption of cement in the United States itself has steadily increased since the 2008 Recession, reaching approximately 102 million metric tons in 2019. It is projected that the global Cement Market is anticipated to rise from USD 340.61 billion in 2022 to USD 481.73 billion by 2029 at a considerable rate during next few years as the cement is counted among the key building materials both in the residential and the nonresidential sector.



Figure 1: Global cement market size (2018-2029)

1.1 CEMENT PROCESS BACKGROUND

Cement is a binder that can bind other materials together, most often sand and gravel, and is then used for construction. When cement is mixed with fine aggregate or with sand and gravel, it produces concrete. Cement can be characterized as hydraulic or non-hydraulic, where non-hydraulic does not set when there is water present, contrary to hydraulic cements, such as Portland cement[1]. It is the most common type of cement named after isle of Portland off coast of England. Most Portland cement is made in a rotary kiln.

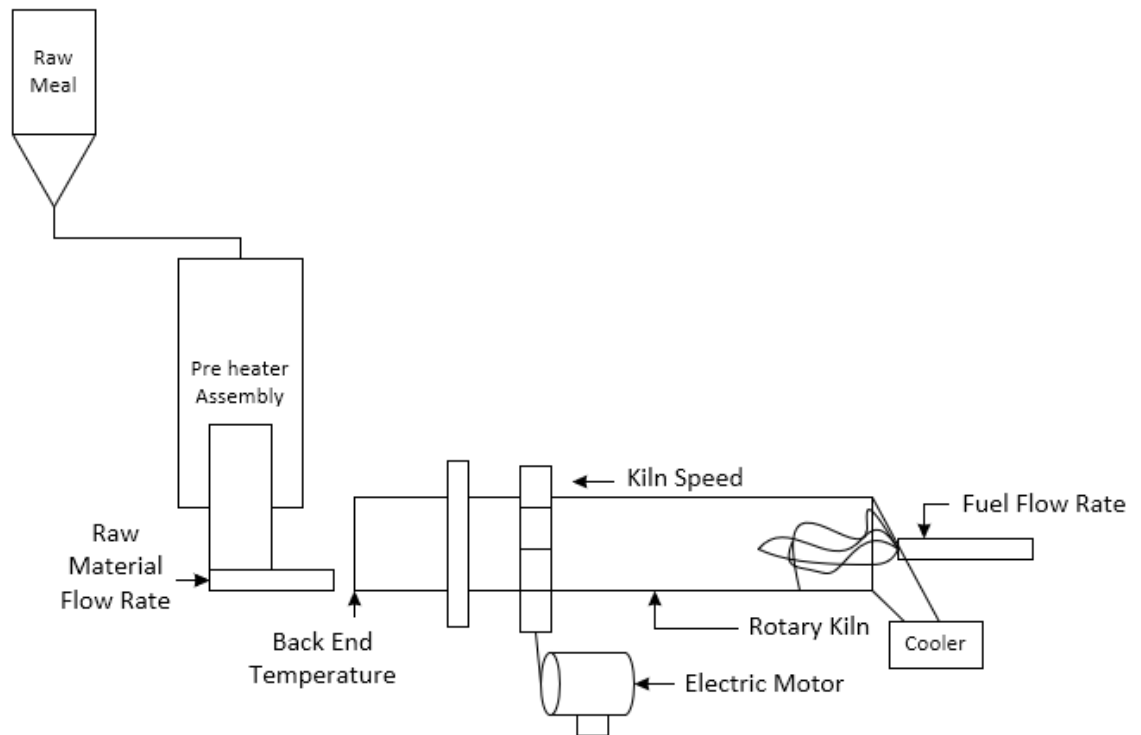


Figure 2: A production scale cement plant

A visual representation of a rotary cement plant is shown in Figure 2. Cement rotary kiln is the most vital part of a cement factory whose output is good quality cement clinker. A rotary kiln is a cylinder with a length of around 70 meters and a diameter of around 5 meters in a factory with a capacity of producing about 2000 tons of clinker in a day. The

kiln is rotated by a powerful electrical motor. The temperature in the hottest point in the kiln is up to 1400°C.

The cement process as shown in Figure 2 begins with the mining of limestone, clay, and other particles. These large blocks are crushed, ground, and mixed with other minerals. The mix is conveyed into the kiln at temperatures approaching ~1500 – 1700°C, where it is transformed into small granules known as clinker. Clinker is ground with gypsum to become a fine powder known as cement[2]. The production of clinker is the most energy intensive process in the cement manufacturing which utilizes approximately 80% of thermal energy. Hence it is important to maintain quality of clinker by reducing energy consumption as well as CO_2 emission.

Several complex processes have been involved in cement production that takes place at extreme high temperatures. Consequently, after transportation and energy, cement production is the third biggest source of carbon dioxide emissions which represents about 6-7% of global anthropogenic CO_2 emissions with the highest thermal energy consumption in the world[3]. It has significant impacts at all stages of process on environment include disturbance to the landscape, dust, noise, and disruption to local biodiversity from quarrying limestone, depletion of natural resources as well as health and safety of people[4].

The ultimate goal of a kiln is to produce clinker of a consistent quality with minimum energy consumption. There are three different zones in the dry cement kiln process: heating zone, burning zone, and cooling zone. The burning zone is the hottest region of the kiln. In this region, temperatures around 1500°C induce the calcium oxide to react with the raw material to form the clinker[5]. As it directly affects the quality of the clinker, it is

extremely important to maintain the nominal operating burning zone temperature (*BZT*) and avoid fluctuations. Also, due to the dusty nature of the clinker within the kiln, existing measurement technologies do not provide the accuracy required to directly measure the *BZT* within the kiln. Measuring the *BZT* is further made difficult as the kiln is rotating at 1 to 3 [RPM][6].

Another important factor is maintaining the kiln torque[7]. A large heavy cylinder with substantial amount of material is rotated with motor-drive system. In this case, starting of the kiln requires high torque that can be 2.5 times the full load torque and in order to avoid damaging the drive gears of the kiln, motor speed and torque synchronization is necessary. In order to create good quality clinker, accurate control on the material flow, so that the burner flame has enough time to heat the raw mix to high enough temperature is extremely important. Depending upon application, high, medium and low voltage, AC-DC Drives system is widely used which can accurately synchronize motor speed and torque[8].

The rotary kiln torque can be affected by many things such as clinker viscosity, burning zone temperature, kiln speed etc. If the clinker is too sticky, it will be adhesive to the kiln lining and go up with the kiln rotation and high motor torque is required to push the material up. Difference in the kiln speed and kiln feed can generate high torque. Hence knowledge of kiln torque is important.

1.2 CURRENT CONTROL/OBSERVATION STRATEGIES FOR ROTARY KILN

In this section, advanced control schema found in the literature is detailed. These papers represent kiln control approaches that utilize advanced methods from research labs and academia. In the process of cement production, the rotary kiln calcination

and clinkerisation is the most important process and includes complicated physical and chemical reactions with large inertia, pure hysteresis, nonlinearity, and strong coupling characteristics[9]. Currently, the cement rotary kilns are mainly controlled manually or semi-automatically, based on the experience of operators and based on past kiln performance. Recently, various control strategies, such as the application of PID neuron networks, have been applied to real-time monitoring, analysis, and optimization of cement kiln control through field bus technology. MPC (Model Predictive Control) strategies were chosen for its straightforward applicability to large, multivariable processes, and its ability to handle constraints, and thus well suited for industrial applications[10].

Researchers presented a study of the application of PID neuron networks to the real-time monitoring, analysis and optimization through the field bus technology to conventional cement production[11]. This work presents the application of PID neuron networks as controllers to control the temperature and pressure of a rotary cement kiln. This work has simulation results based on MATLAB/SIMULINK and it concludes that the presented method can reach satisfactory performance by online learning and self-adjusting without establishing accurate mathematical model and independent on the model identification[12]. Researchers also report that Model Predictive Control (MPC) techniques have been adopted for controlling the rotary cement kiln unit. A mathematical model of the process in was developed to capture the dynamic relationships between the variables of the system[13, 14]. This model is used to predict the evolution of the process to possible future control characteristics. Among all the trajectories capable to maintain process variables within the limitations assigned, the one that provides the best performance in term of minimization of a cost function is computed. Researchers have

developed a fuzzy advising control unit to improve clinker quality and to reduce energy consumption in a rotary cement kiln[15]. This system is based on sintering zone state assessment, the kiln rotation period and the relative change of the exhaust gases temperature. Structure of fuzzy control system is proposed, and it is based on advising control unit. It is applicable as both an independent system and as a part of the existing rotary kiln control systems[16].

It is seen that multi-physics tools that are core to modern engineering and smart manufacturing are not very popular nor are widely used in the cement industry. Considering this fact, there are significant opportunities to seek methods to reduce reliance on physical sensors and instead develop physics based analytical methods to aid the kiln control. Hence, using nonlinear observation scheme using theory-based approach along with the data centric approach using Multiphysics tool is being explored in this dissertation in the respective sections.

1.3 MOTIVATION FOR RESEARCH

Modeling entire rotary kiln from feed end to discharge end will require the discretization of the entire space, material, refractory walls etc. which is costly and unnecessary. The full-blown analytical model using Multiphysics modeling tool with the thermodynamics, chemical reactions can give us computationally intensive model and cannot be used in the real time observations of the burning zone. Also, it will require lots of assumptions which can lead potential inaccuracies in the complete analytical model.

Considering all these challenges with the full-blown analytical model, proposed approach in this dissertation bridges the gap between system theoretic style approach to a data centric approach along with the Multiphysics model. This hybrid approach combines

the Multiphysics model of the lab kiln, equations from multi-physics model and the experimental data from the lab scale kiln to develop the *BZT* observers. Contribution of this dissertation is to take an experimental platform along with the Multiphysics model and from these two things extract a reduced order model that is appropriate for system theory-based approach to develop this observer technique to demonstrate its effectiveness. This approach can be scaled to apply to a real cement kiln in future.

Another challenge while operating the rotary cement kiln is torque control as discussed. A widely accept control variable in the management of the kiln burning zone placement and temperature is the rotational drive system torque. While traditional drive control systems are able to manage the kiln speed without knowledge of load torque, a typical drive will provide an approximate estimator of load torque. These indicators are often approximation or even an off-line measure that has significant error as well as time delay.

In this dissertation, proposed nonlinear observer that provide real-time load torque information that is available for the various aspects of the kiln control system. Proposed nonlinear observer can learn the trajectory of the kiln torque through minimal input information. The torque observer scheme is validated through Lyapunov-based stability analyses and PLECS (a circuit simulation platform) simulation results are obtained which demonstrate the observer viability. This work can be update for any drive type and we will consider induction, synchronous, and hydraulic motors.

1.4 OBJECTIVES

As a part of this approach, the lab kiln is modeled as a series of slices. Proposed nonlinear observers can predict the temperatures and heat rate value in each slice using

both real-time data from temperature sensors along the length of kiln in combination with Multiphysics models. These proposed observers can be used to create virtual sensors for unmeasurable system information currently not available to the process control systems. The process control system can then utilize this information to improve energy efficiency of the process and quality levels of clinker (cement) being produced. For this dissertation, observers utilizing the robust integral of sign of error (RISE) scheme are considered due to the robustness and computational simplicity of this algorithm.

A pair of the real time observers are developed from different temperature measurements within kiln structure. The first of these is the temperature observer for the innermost layer inside the kiln which utilizes the two thermocouple temperature measurements touching outer layers along with the knowledge of the thermal model. The second observer presented in this paper examines the heat rate through wall and utilizes the estimate from temperature observer along with knowledge of thermal resistances and capacitances of the kiln components. This algorithm eliminates the need for costly cameras and pyrometers and can be used to gain exact knowledge of burning zone temperature. Lyapunov-based stability analyses are presented for each observer to prove that all observer signals are bounded and that the respective error signals converge to zero.

As stated, knowledge of the thermal parameters is priori known. Parameter estimation is used to estimate the thermal parameters based on the data and it is further used to validate the parametric information used in Multiphysics model. Once the parameters are known, temperature and heat rate observer are developed. Adaptive least-squares algorithms are commonly used to calculate parameters over a specified interval of samples. In[17], we see how this method can be applied to time-varying parameters in linear systems and [18]

shows an implementation specifically for linear compressors. For this dissertation, an adaptive least-squares algorithm as described in [19] was investigated.

The cascade control structure is selected for permanent magnet DC motor drives because of its flexibility, which consists of distinct control loops, current loop followed by speed loop. Simple PI Controller is designed which manages the kiln speed without knowledge of the kiln torque dynamics, a nonlinear observer is also designed that can discover these dynamics, hence the time-varying load torque in real time. This observer can learn the trajectory of the kiln torque through minimal knowledge.

2. EXPERIMENTAL PLATFORM

A lab scale rotary cement kiln is constructed on the campus for experimental validation of the multi-physics model shown in figure 3. The kiln design is based on a production-scale cement kiln, and it is instrumented with various sensors such thermocouples and pyrometers for acquiring data. The controls system implemented in this project is based on the NI LabVIEW platform with NI cRIO 9064 and Labjack T7-PRO modules serving as hardware interfaces. The main sensors consist of two pyrometers, a speed encoder, and 30-type K, N, C thermocouples. Several experimental trials which culminated into production of cement clinker are conducted to record data that is then utilized to validate the system model and observer design.



Figure 3: Lab scale rotary kiln setup

2.1. PYROMETER LABVIEW INTERFACE

The two Pyrometers (MY 46 and MY 311) are connected to the C – Series current input module. The NI 9203 card is used for this purpose, which supports high performance control and monitoring application. The NI 9203 is a C Series DAQ module with 8 analog current input channels. Input ranges of ± 20 mA or 0 mA to 20 mA, 16-bit resolution, and a 200 kS/s maximum sampling rate were selected to support the pyrometers. This card sends the signal to the host computer for visualization. LabVIEW code is implemented in the LabVIEW FPGA and modified in such a way that both current (mA) and temperature (deg C) can be measured, then it is programmed into National Instruments CompactRIO (cRIO 9064). Block diagram below in Figure 4 shows the Pyrometer-LabVIEW interface.

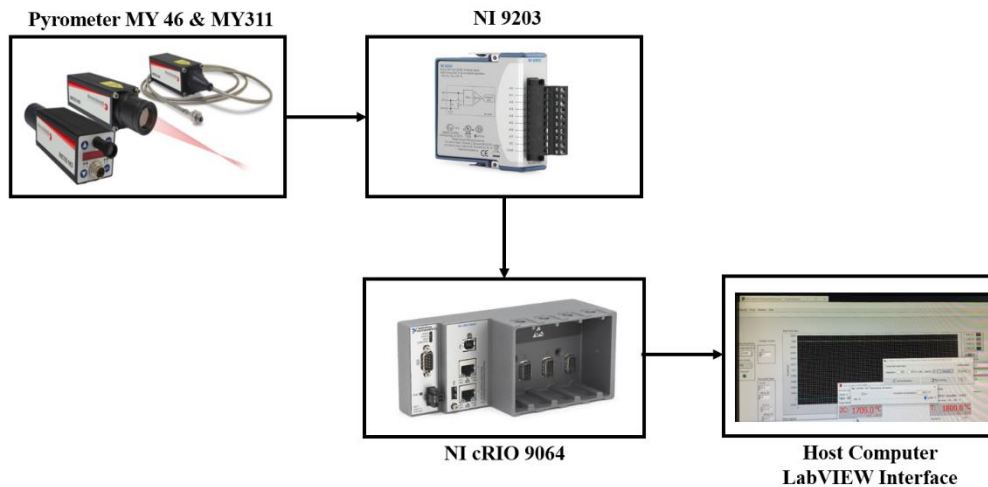


Figure 4: Pyrometer-LabVIEW Interface

2.2 THERMOCOUPLE - LABJACK INTERFACE

For the lab scale kiln, different types of thermocouples such as C-type, N-type and K-type are used to acquire temperature data during experimental test runs. Total 30

thermocouples are located at various locations such as touching alumina tube, potting compound, and the kiln shell measuring temperatures more accurately. These thermocouples are connected to analog input channels of Labjack T7 module and mounted inside the enclosure along with Expansion board, two CB37 terminal boards, battery and connected using 3ft DB37 M/F serial cable. Hence the enclosure dimensions are chosen approximately 15.3x12.13x6.47 (numbers are in inches) to fit all the components onto the lab kiln. The real-time temperature measurement is done using data acquisition in LabVIEW. Since the lab scale kiln is rotating, wireless data logging system is selected which can record the data every after 10 seconds interfaced with LabVIEW over WiFi. Figure 5 below shows the general connection diagram inside the enclosure.

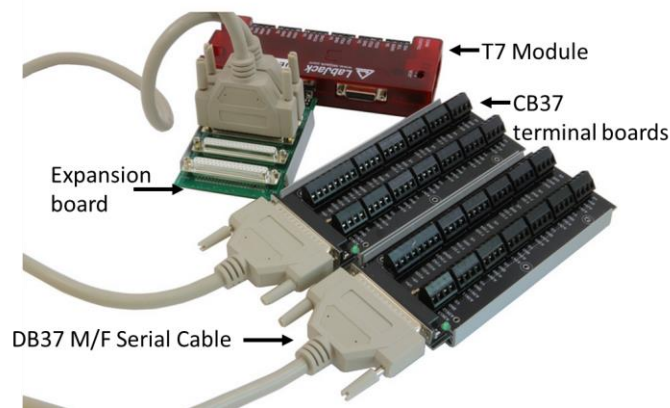


Figure 5: Labjack assembly inside the enclosure for temperature measurement

2.3 Mass Flow Controller

The thermal mass flow device provides an accurate, fast and convenient gas measurement and control. There are two controllers. These thermal mass flow controllers are connected the NI- cRIO 9064 with analog input and output card for real time data measurement. Figure 6 represents the connection diagram of the controller unit. The

controller has unipolar power supply and 4-20mA signals. These analog inputs are configurable via digital communications and internal jumper settings. The analog inputs can be a voltage while the output is current, or vice versa. The standard analog output of the flow meter is a 0-5 VDC signal proportional to the flow rate.

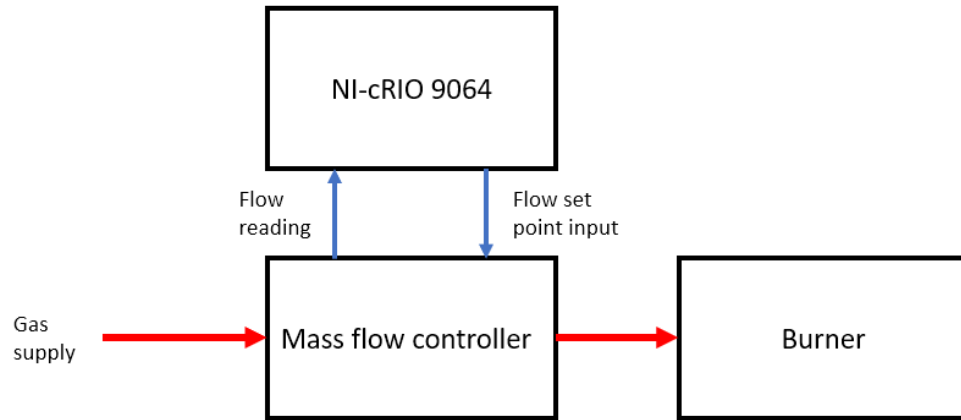


Figure 6: Mass flow controller connection with cRIO 9064

2.4 LAB SCALE KILN TEST RESULTS

Multiple rounds of tests were carried out on the lab scale kiln. The initial tests were focused on debugging the setup and data acquisition. In final few rounds, the tests culminated in production of clinker with each round lasting over 9 hours. In these rounds, the first part involved heating the stationary kiln to $>1000^{\circ}\text{C}$ and took about 5 hours. Once the kiln reached adequate temperature, meal was fed, and kiln was rotated at 1-2RPM to produce clinker. Data was recorded throughout heating as well as clinker production phase and is showcased in the graphs below. The graphs (Figure 7- Figure 12) show temperature data from 30 thermocouples, pyrometer data, and kiln surface temperature data. This temperature data was then used in the design of burning zone temperature observer.

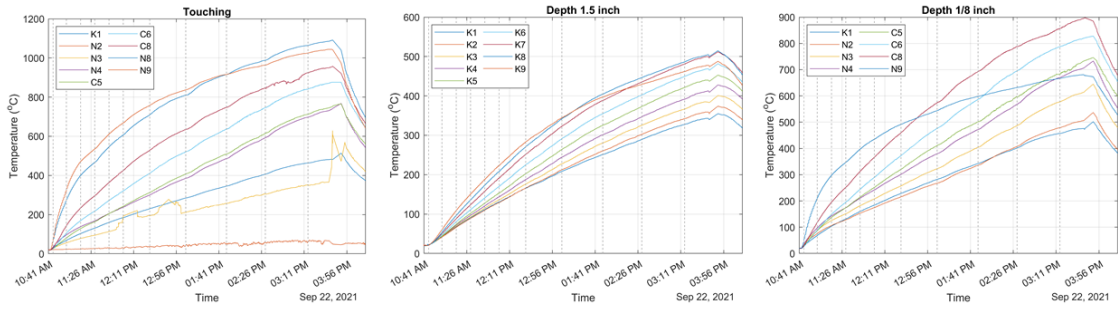


Figure 7: Test run results (09/22/2021)

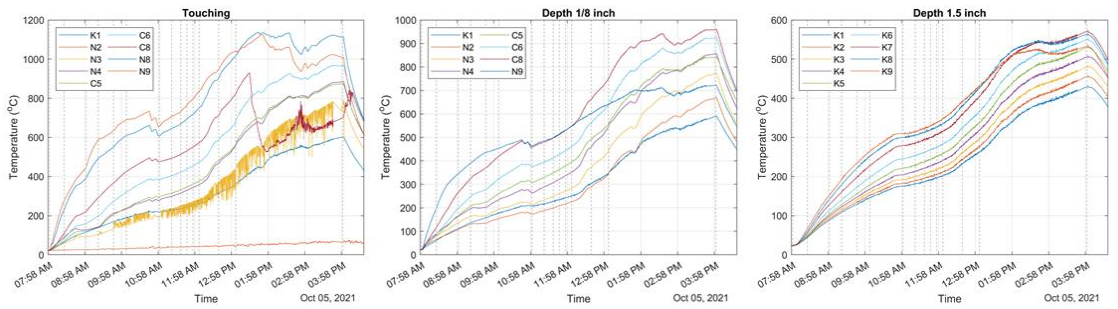


Figure 8: Test run results (10/05/2021)

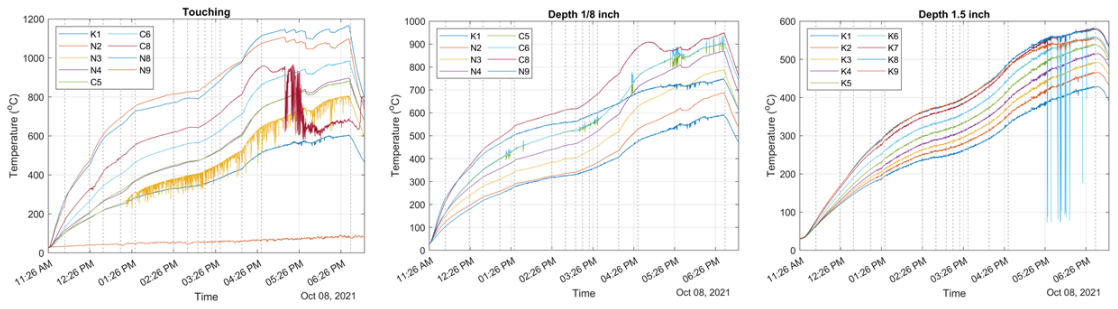


Figure 9: Test run results (10/08/2021)

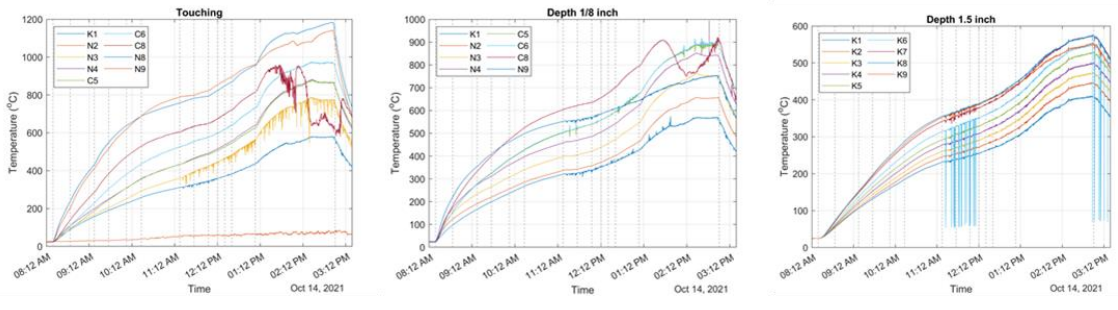


Figure 10: Test run results (10/14/2021)

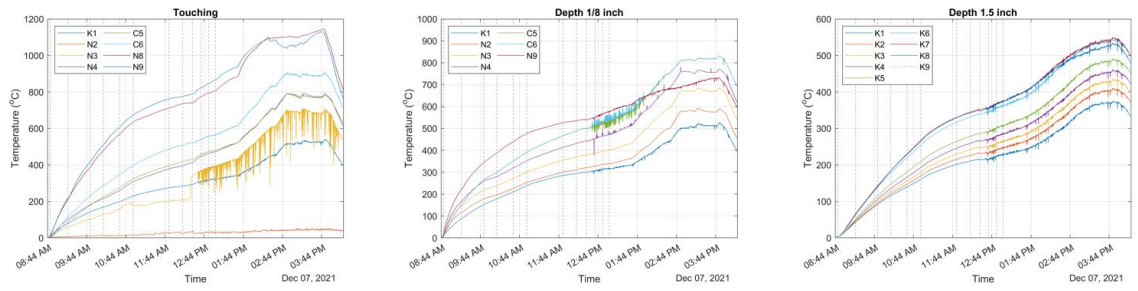


Figure 11: Test run results (12/07/2021)

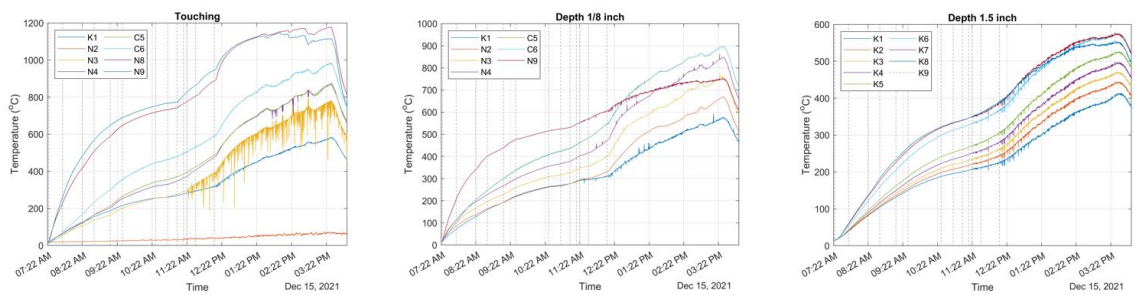


Figure 12: Test run results (12/15/2021)

Figure 13 represent the pyrometer temperature at the time of material flowing through the kiln. It also has burning zone temperature recorded. Down spikes are because of pyrometer was moved while using carbon rod.

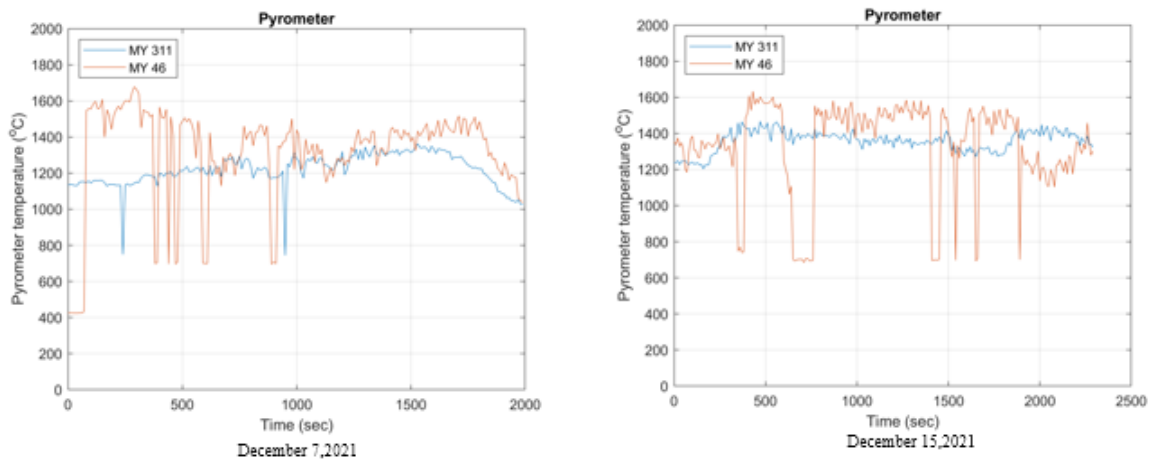


Figure 13: Pyrometer temperature profile

Figure 14 represent the temperature profile of the 30 thermocouples at the time of material flowing through the kiln. This data will be further used to design and validate burning zone observer.

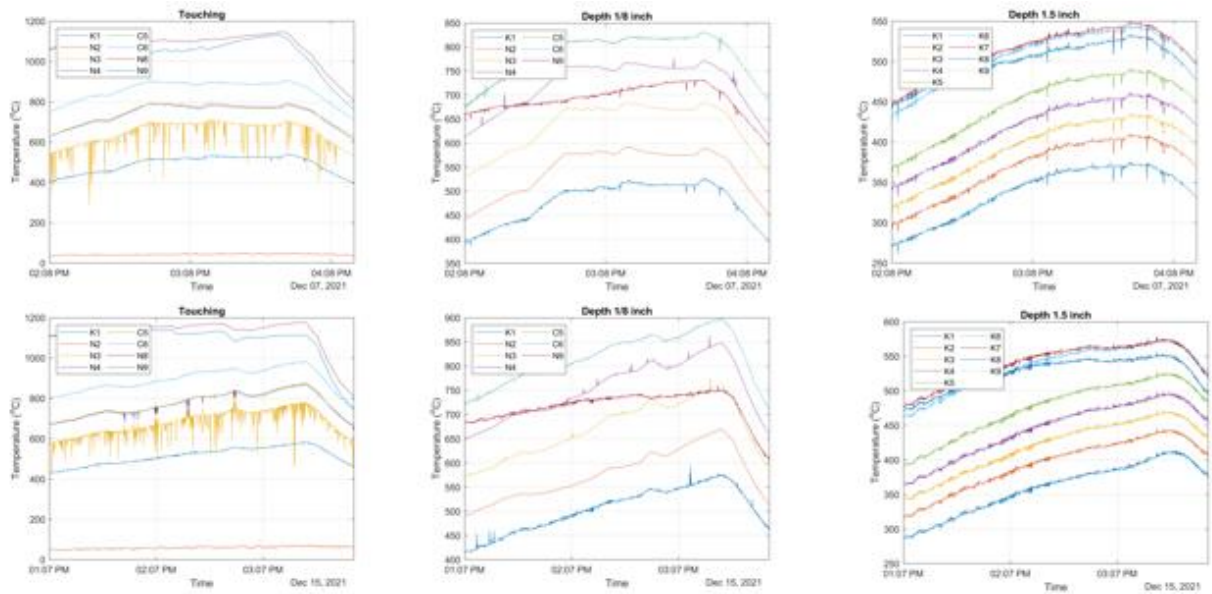


Figure 14: Temperature plot at the time material flowing through the kiln

3 REDUCED OREDR THERMAL MODEL APPROACH

The proposed approach is based on lumped thermal interface that finds the relation between real-time data and the multi-physics model. The lumped thermal system interface is used to reduce system's complexity by replacing portions of it with equivalent circuit elements and then it is informed by multi-physics for its material properties. Using various temperature sensor data and fuel/heat rates, burning zone temperature observer is then developed, designed and validated using a lab scale kiln.

The heat loss to the surroundings through the kiln wall can be modeled with a thermal circuit analogous to an electrical circuit. The burner introduces heat at one end of the kiln and the gases carry it along the length of the kiln. Through the process, some of this energy is expended in carrying out the chemical reactions that produce cement while some energy is lost to the surroundings through the kiln wall. Since the problem is 3D in cylindrical coordinate system, the kiln can be imagined as series of slices along its axis. Each such slice will have a different radially outward heat flow rate with slices closest to the burner having the highest magnitude. Subsequently, the radial temperature profile along the layers will be different at each slice. Figure 15 below shows an illustration of this. As a simplification for the sake of discussion below, one of such slices is being modeled as with a single heat transfer rate to get a singular radial temperature profile. The simulated data will then be compared with measurement data.

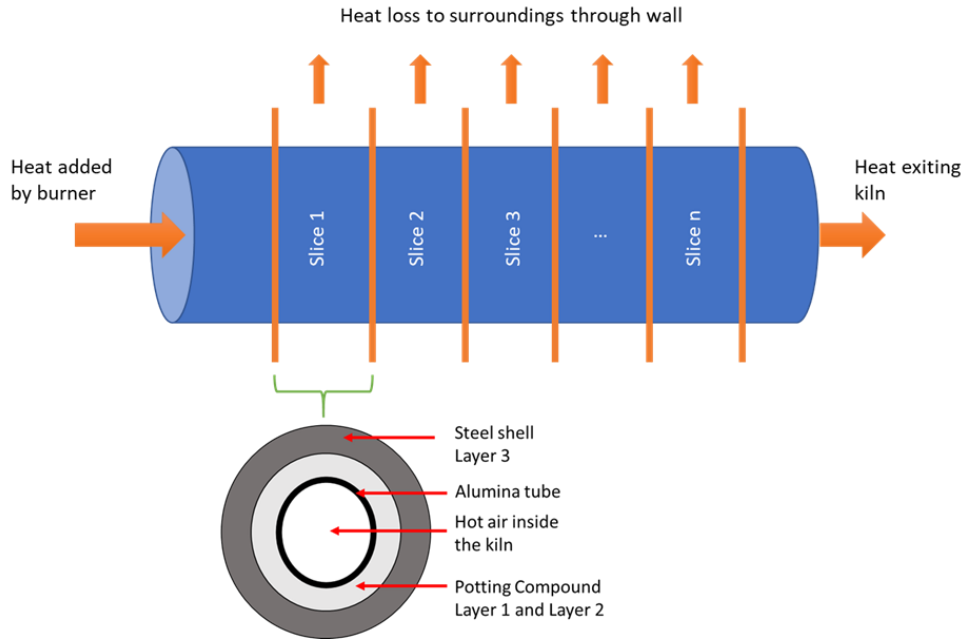


Figure 15: Illustration for modeling kiln as slices

Figure 16 represents the three radial layers of the lab scale kiln enclosure being labeled as L_1 , L_2 and L_3 . L_1 and L_2 layers are of potting compound whereas L_3 is the kiln steel shell. $T_1(t)$, $T_2(t)$, and $T_3(t)$ are the temperatures in $^{\circ}\text{C}$ measured by different types of temperature sensors such as C-type, N-type, and K-type thermocouples, respectively at different length of the kiln as shown in Fig 16.

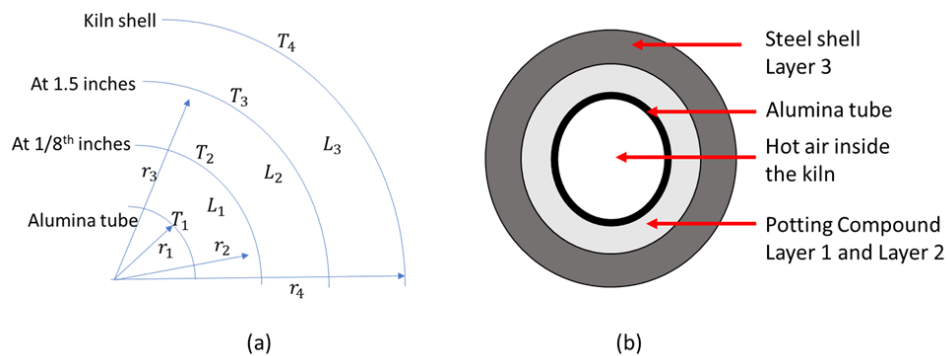


Figure 16: 2-D model and cross section of the kiln representing different layers and thermocouple position

Temperature of the kiln's steel shell is measured by an IR camera and is represented by $T_4(t)$. r_1 is the inner radius of alumina tube, r_2 is the outer radius of alumina tube, which is same as inner radius of potting material, r_3 is the outer radius of the potting material which is same as inner radius of steel shell and r_4 is the outer radius of steel shell. With the geometry in place, the layers can then be modeled as thermal resistors and capacitors. To think in terms of energy flow, a certain amount of energy leaves from the kiln center. A part of it will be expended in heating first layer (thermal mass = thermal capacitance). The remainder will overcome layer 1 thermal resistance and reach layer 2 and so on. That yields the following thermal circuit where C_x are thermal capacitances and R_x are thermal resistances of any given layer x in SI units (K/W for thermal resistance, J/K for thermal capacitance). Figure 17 represents the thermal-electrical analogy for conduction heat transfer for the kiln.

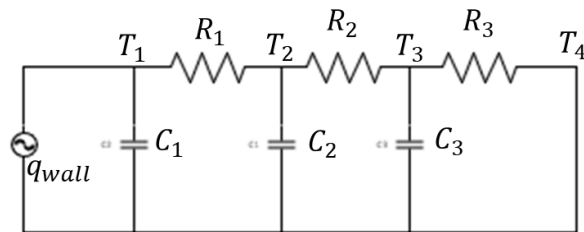


Figure 17: Thermal resistance and capacitor network

The resistances and capacitances for any given layer x can be calculated using the following:

$$R_x = \frac{\ln(r_{out}/r_{in})}{2\pi L k_x} \quad (1)$$

$$C_x = \pi(r_{out}^2 - r_{in}^2)L\rho_x C_{px} \quad (2)$$

where L is length of the slice being modeled in meter, ρ is density of the layer in $[\text{kg}/\text{m}^3]$, k is thermal conductivity in $\text{W}/\text{m}\cdot\text{K}$, and C_p is the specific heat capacity of the layer in $\text{J}/\text{kg}\cdot\text{K}$. Furthermore, r_{out} and r_{in} are the outer and inner radii for any given layer in meters.

The governing time dependent differential equations for this circuit are as below

$$q_{wall} = (T_1 - T_2)/R_1 + C_1 \frac{dT_1}{dt} \quad (3)$$

$$(T_1 - T_2)/R_1 = (T_2 - T_3)/R_2 + C_2 \frac{dT_2}{dt} \quad (4)$$

$$(T_2 - T_3)/R_2 = (T_3 - T_4)/R_3 + C_3 \frac{dT_3}{dt} \quad (5)$$

where q_{wall} is the heat transfer rate through the slice in watts, R_1 , R_2 , R_3 are thermal resistances of layers 1, 2 and 3 respectively and C_1 , C_2 , C_3 are thermal capacitances of layers 1, 2 and 3 respectively. This linear system of first order ordinary differential equations (3), (4), and (5) are solved using MATLAB.

3.1 THERMAL PARAMETER ESTIMATION

In an effort to create a valid reduced order model, our validated Multiphysics model is utilized here to determine our parametric information for a given slice. An adaptive least-squares estimator is to be developed for estimation of the thermal parameters of the lab scale kiln single slice presented in Section II. This strategy is used to connect the real time data to the Multiphysics model to the reduced order model presented in section II. For the proceeding mathematical analysis, the following assumptions are made.

Assumption 1: The parameters $R_1, R_2, C_1,$ and C_2 are unknown and constants. $T_1(t), T_2(t)$ being slowly time varying such that $\dot{T}_1(t) \approx 0, \dot{T}_2(t) \approx 0$.

Assumption 2: The variables such that $T_1(t), T_2(t), \dot{T}_1(t), \dot{T}_2(t)$ are all piecewise continuous and bounded with exception of $\dot{T}_1(t), \dot{T}_2(t)$ are measurable

Assumption 3: The initial conditions of all the variables are not equal to zero. Estimation begins at ambient temperature.

Assumption 4: $q_{wall}(t)$ is known *priori* and exported from COMSOL.

An adaptive least-squares estimator for the unknown thermal parameters is to be designed utilizing dynamic eq (3). To facilitate the estimator development this equation is rewritten along with constants and variables as follows:

$$a_m = W\theta \quad (6)$$

Where, $a_m(t) \triangleq \dot{T}_1(t)$ and $W \triangleq [W_1 \quad W_2] \in \mathbb{R}^{1 \times 2}$ is the known regression vector.

Where $W_1(t), W_2(t) \in \mathbb{R}$ are defined as follows

$$W_1 \triangleq q_{wall} \quad (7)$$

$$W_2 \triangleq T_2 - T_1 \quad (8)$$

In (6), $\theta \triangleq [\theta_1 \quad \theta_2]^T \in \mathbb{R}^2$, is the parameter vector with the elements defined as follows:

$$\theta_1 \triangleq \frac{1}{C_1} \quad (9)$$

$$\theta_2 \triangleq \frac{1}{R_1 C_1} \quad (10)$$

To facilitate the estimator design, a prediction error $\varepsilon(t)$ is defined as follows

$$\varepsilon \triangleq \hat{a}_f - a_f \quad (11)$$

Where a_f is the filtered temperature of the alumina tube and is defined as follows

$$\dot{a}_f \triangleq -\beta_o a_f + \beta_o a_m \quad (12)$$

Where $a_f(t_0) = 0$ and $\beta_o > 0$ constant. In (11), $\hat{a}_f(t)$ is the estimate of filtered temperature defined as follows:

$$\hat{a}_f \triangleq W_f \hat{\theta} \quad (13)$$

Where $W_f \in \mathbb{R}^{1 \times 2}$ is the filtered regression vector, defined as follows:

$$\dot{W}_f \triangleq -\beta_o W_f + \beta_o W \quad (14)$$

Where $W_f(t_0) = [0 \ 0]$ and β_o was introduced in (12). In (13), $\hat{\theta}(t) = [\hat{\theta}_1 \ \hat{\theta}_2]^T \in \mathbb{R}^2$ is the estimate vector of unknown parameters. From (6), (12) and (14) it is possible to write the following expression

$$\dot{a}_f + \beta_o a_f = \dot{W}_f \theta + \beta_o W_f \theta \quad (15)$$

The estimated parameter error signal defined as follows

$$\tilde{\theta} \triangleq \theta - \hat{\theta} \quad (16)$$

Where $\tilde{\theta}(t) \in \mathbb{R}^2$.

An unmeasurable form of prediction error $\varepsilon(t)$ can be written as follows

$$\varepsilon \triangleq W_f \tilde{\theta} \quad (17)$$

From the error signal continuous-time least-square update law can be developed as follows

$$\dot{\hat{\theta}} = -K_{ls} \frac{P_{ls} W_f^T \varepsilon}{1 + \gamma W_f P_{ls} W_f^T} \quad (18)$$

Where K_{ls} is constant diagonal matrix, γ is positive constant gain, $\varepsilon(t)$ was defined in (11), W_f was defined in (14), $P_{ls}(t)$ is a covariance matrix. The matrix $P_{ls}(t)$ is generated by the covariance propagation equation which is described as follows

$$\dot{P} = -K_{ls} \frac{P_{ls} W_f^T W_f P_{ls}}{1 + \gamma W_f W_f^T} \quad (19)$$

Where $P_{ls}(t_0) = k_o I, k_o \in \mathbb{R}^+$. is a constant gain and $I \in \mathbb{R}^{2 \times 2}$. Is the standard 2×2 identity matrix. The estimated parameters of the thermal circuit is defined as follows:

$$C_1 = \frac{1}{\hat{\theta}_1}, \frac{1}{R_1} = \frac{\hat{\theta}_2}{\hat{\theta}_1} \quad (20)$$

Similarly, an adaptive least-squares estimator for the unknown thermal parameters is to be designed utilizing dynamic eq (4).

Remark: From (20) it is clear that special care needs to be taken to avoid $\hat{\theta}_1(t) = 0$. To achieve this condition, the projection algorithm described in [] must be utilized. This algorithm takes into account $\hat{\theta}_1(t)$ and $\dot{\hat{\theta}}_1(t)$ to keep $\hat{\theta}_1(t) > 0$, while maintaining stability and convergence of the least-squares estimation strategy.

Theorem 3.1: The least-squares algorithm described by (18) and (19) ensures that $\tilde{\theta} \rightarrow 0$ as $t \rightarrow \infty$, provided the following sufficient conditions are met: 1) the plant of estimation is strictly proper; 2) the input is piecewise continuous and bounded; 3) the output of the plant of estimation is bounded;

and 4) the following persistence of excitation condition holds:

$$\beta_1 I \leq \int_{t_0}^{t+\delta} W_f^T(\tau) W_f(\tau) d\tau \leq \beta_2 I \quad (21)$$

Where $\beta_1, \beta_2, \delta \in \mathbb{R}^+$ are constants and $I \in \mathbb{R}^{2 \times 2}$, Is the standard 2×2 identity matrix.

Proof: To prove that $\tilde{\theta} \rightarrow 0$ as $t \rightarrow \infty$, Theorem 2.5.3 from [18] is followed directly.

Condition 1) is proved to be valid as the plant of estimation described in (8) can be seen to be strictly proper. Condition 2) is met by recognizing that the reference input to the plant $a_m(t)$ is solely dependent upon the signal $\dot{T}_1(t)$ which as stated in Assumption 2 is

bounded and piecewise continuous. Condition 3) is met by utilizing standard linear analysis tools it can be shown that since $a_m(t)$ is bounded $a_f(t), \dot{a}_f(t) \in \mathcal{L}_\infty$. Condition 4) is dependent on the way in which the system is excited.

3.2 BURNING ZONE TEMPERATURE AND HEAT RATE OBSERVER

DEVELOPMENT

3.2.1. ALUMINA TUBE TEMPERATURE OBSERVER DEVELOPMENT ($\hat{T}_1(t)$)

In previous section, a scheme was developed which allowed for the thermal parameters in (3-5) for a given slice to be synchronized between the real time experimental data and the Multiphysics model. In this section two observers are developed utilizing the general form of the reduced order models for a given slice. In this section the first observers approximate the unmeasurable burning zone, $T_1(t)$ with in a given slice of the lab kiln. Using and the dynamic model in (4), a real time observer for $T_1(t)$ is developed. This observer will not use measured value for T_1 but utilizes other measurements $T_2(t)$, $T_3(t)$, $T_4(t)$. For lab scale kiln this can make observer using vectors and matrices for every slice at same time. To facilitate the development of the temperature observer, (4) can be rewritten as.

$$\dot{T}_2 = \frac{T_1 - T_2}{R_1 C_2} - \frac{T_2 - T_3}{R_3 C_3} \quad (22)$$

The nonlinear observer to be designed for the signal $T_1(t)$ is denoted as $\hat{T}_1(t) \in \mathbb{R}$. For a given $\hat{T}_1(t)$, (22) can be utilized to obtain an observation for $\dot{T}_2(t)$ represented as

$$\dot{\hat{T}}_2 = \frac{\hat{T}_1}{R_1 C_2} - \frac{T_2}{R_1 C_2} - \frac{T_2}{R_3 C_3} + \frac{T_3}{R_3 C_3} \quad (23)$$

Temperature observer error term can be defined as follows

$$e_{T_2} = T_2 - \hat{T}_2 \quad (24)$$

Such that $e_{T_2} \rightarrow 0$ as $t \rightarrow \infty$. In an effort to complete the design, the time derivative of (24) is taken and can be written as follows

$$e_{T_2} \dot{=} \dot{T}_2 - \dot{\hat{T}}_2 \quad (25)$$

A filtered error signal can be defined as

$$s_{T_2} = e_{T_2} \dot{=} + e_{T_2} \quad (26)$$

From the subsequent stability analysis, the following observer is designed

$$\dot{\hat{T}}_1 = [(k_1 + 1)s_{T_2} + k_2 \cdot \text{sgn}(e_{T_2})] \quad (27)$$

Where $k_1, k_2 \in \mathbb{R}^+$, are constant gains, $\text{sgn}(\cdot)$ is the signum function. The dependence of (27) on $s_{T_2}(t)$ makes it unrealizable. A realizable form of $\hat{T}_1(t)$ can be obtained by substituting (26) into (27) and integrating both sides of the resulting equation to obtain the following:

$$\begin{aligned} \hat{T}_1 = (k_1 + 1) & \left[e_{T_2}(t) - e_{T_2}(t_0) + \int_{t_0}^t e_{T_2}(\sigma) d\sigma \right] \\ & + k_2 \left[\int_{t_0}^t \text{sgn}(e_{T_2}(\sigma)) d\sigma + \hat{T}_1(t_0) \right] \end{aligned} \quad (28)$$

3.2.2. EQUIVALENT HEAT SOURCE OBSERVER DEVELOPMENT ($\hat{q}_w(t)$)

Validated reduced order model with parameters is established in the sections above. Using this information, effective heat value is extracted further in this section. Once there is an estimate for $T_1(t)$, then using eq 3 the effective heat value of q_{wall} is observed. q_w is the equivalent heat source inside a given slice like current source. Using combination of observers for a given slice (using eq 4 and eq (3)) $\hat{q}_w(t)$ is developed. To facilitate the development of the heat source observer, (3) can be rewritten as

$$\dot{T}_1 = \frac{q_w}{c_1} - \frac{T_1 - T_2}{c_1 R_1} \quad (29)$$

The nonlinear observer to be designed for the signal $q_{\text{wall}}(t)$ is denoted as $\widehat{q}_w(t) \in \mathbb{R}$. For a given $\widehat{q}_w(t)$, (29) can be utilized to obtain an observation for $\dot{T}_1(t)$ represented as

$$\dot{\widehat{T}}_1 = \frac{\widehat{q}_w}{c_1} - \frac{T_1 - T_2}{c_1 R_1} \quad (30)$$

Heat rate observer error term can be defined as follows

$$e_{T_1} = T_1 - \widehat{T}_1 \quad (31)$$

Such that $e_{T_1} \rightarrow 0$ as $t \rightarrow \infty$. In an effort to complete the design, the time derivative of (31) is taken and can be written as follows

$$e_{T_1}^{\dot{}} = \dot{q}_w - \dot{\widehat{q}}_w \quad (32)$$

A filtered error signal can be defined as

$$s_{T_1} = e_{T_1}^{\dot{}} + e_{T_1} \quad (33)$$

From the subsequent stability analysis, the following observer is designed

$$\dot{\widehat{q}}_w = [(k_{11} + 1)s_{T_1} + k_{22} \text{sgn}(e_{T_1})] \quad (34)$$

Where $k_{11}, k_{22} \in \mathbb{R}^+$, are constant gains, $\text{sgn}(\cdot)$ is the signum function. The dependence of (34) on $s_{T_1}(t)$ makes it unrealizable. A realizable form of $\widehat{T}_1(t)$ can be obtained by substituting (33) into (34) and integrating both sides of the resulting equation to obtain the following:

$$\begin{aligned} \widehat{q}_w = (k_1 + 1) & \left[e_{T_1}(t) - e_{T_1}(t_0) + \int_{t_0}^t e_{T_1}(\sigma) d\sigma \right] \\ & + \left[k_2 \int_{t_0}^t \text{sgn}(e_{T_1}(\sigma)) d\sigma + \widehat{q}_w(t_0) \right] \end{aligned} \quad (35)$$

3.2.3 STABILITY ANALYSIS

Remark: Given that the form of the observers defined in (28) and (35) and their corresponding error (24)–(26) and (31)–(33) are identical and a single stability analysis is given for both. The subscript k used in the subsequent analysis may be replaced with a T_1 or q_w to refer to terms in the alumina tube temperature or heat rate observers, respectively. All equations from the observer developments referenced herein use one citation for each observer with the burning zone temperature observer being referenced first (e.g., $(T_1 \#/q_w \#)$)

Theorem 1: The observer in (35) ensures that $e_k(t), S_k(t) \rightarrow 0$ as $t \rightarrow \infty$.

Proof: The stability of closed loop system presented by (35) can be shown through a non-negative Lyapunov function $V_o(t) \in \mathbb{R}$ defined as

$$V_o = \frac{1}{2} e_k^2 + \frac{1}{2} s_k^2. \quad (36)$$

Taking derivative of equation (16)

$$\dot{V}_o = e_k \dot{e}_k + s_k \dot{s}_k. \quad (37)$$

On solving (26) for \dot{e}_{ω_m} and substituting it alongside (27) and simplifying yields

$$\dot{V}_o = s_k^2 - e_k^2 + s_k (\dot{T}_1 - \hat{T}_1). \quad (38)$$

Substituting in (49) into (38) and rearranging eventually yield

$$\begin{aligned} \dot{V}_o = & -e_k^2 - k_1 s_k^2 + \dot{e}_k \hat{T}_1 - \dot{e}_k k_2 \operatorname{sgn}(e_k) \\ & + e_k (\dot{T}_1 - k_2 \operatorname{sgn}(e_k)) \end{aligned} \quad (39)$$

Integrating both sides of equation (39) gives

$$V_o = V_o(t_f) + A_1 - A_2 + A_3 - A_4. \quad (40)$$

where,

$$A_1 = \int_{t_o}^t (\dot{e}_k(\sigma)\dot{T}_1(\sigma)d\sigma). \quad (41)$$

$$A_2 = k_2 \operatorname{sgn}(e_k) \int_{t_o}^t (\dot{e}_k(\sigma)d\sigma). \quad (42)$$

$$A_3 = \int_{t_o}^t e_k(\sigma) [\dot{T}_1(\sigma) - k_2 \operatorname{sgn}(e_k(\sigma))] d\sigma. \quad (43)$$

$$A_4 = \int_{t_o}^t (e_k^2(\sigma)d\sigma + k_1 \int_{t_o}^t s_k^2(\sigma)d\sigma). \quad (44)$$

And $V_o(t_f)$ is the final value of V_o . Using integration by parts on equation (41) yields

$$A_1 = (e_k(t)\dot{T}_1(t) - e_k(t_o)\dot{T}_1(t_o) - \int_{t_o}^t e_k(\sigma)\ddot{T}_1(\sigma)d\sigma). \quad (45)$$

And evaluating (42) yields

$$A_2 = k_2 \operatorname{sgn}(e_k(t))e_k(t) - k_2 \operatorname{sgn}(e_k(t_o))e_k(t_o). \quad (46)$$

Substituting equations (44), (45) into (40) and simplifying yields

$$V_o \leq - \int_{t_o}^t e_k^2(\sigma)d\sigma - k_1 \int_{t_o}^t s_k^2(\sigma)d\sigma + C. \quad (47)$$

where,

$$C = V_o(t_f) - e_k(t_o)[\dot{T}_1(t_o) - k_2 \operatorname{sgn}(e_k(t_o))]$$

Since C is a constant, the derivative yields

$$V_o \leq -e_k^2 - k_1 s_k^2. \quad (48)$$

which is negative definite all time.

Since equation (36) ≥ 0 and (48) ≤ 0 , for all time t , it can be said that $e_k(t), S_k(t) \in \mathcal{L}_\infty \cap \mathcal{L}_2$. From this it is also said that from (26) that $\dot{e}_k \in \mathcal{L}_\infty$. From the form of (27) it is then proved that $\dot{T}_1 \in \mathcal{L}_\infty$. Looking at (26), using *Assumption 2* it can be said

that $\dot{s}_k \in \mathcal{L}_\infty$. Since $e_k, \dot{e}_k, s_k, \dot{s}_k \in \mathcal{L}_\infty$, then according to Barbalat's Lemma can be proved that $|e_k(t)|, |s_k(t)| \rightarrow 0$ as $t \rightarrow \infty$.

3.3 EXPERIMENTAL RESULTS

3.3.1 THERMAL CIRCUIT PARAMETER ESTIMATION

The parameter estimator described in (18) and (19) was implemented on the simulation platform under the conditions stated. The thermal parameters represent the physical properties of the material and can significantly affect the thermal behavior of the system. Real-time measurements for the thermocouple temperatures $T_2(t)$, $T_3(t)$, $T_4(t)$ are used from the test result carried out on Oct 14th, 2021. Gain values of $\gamma = 100$, $k_1 = 0.1$, and $k_2 = 0.01$ were selected via trial and error for optimal convergence and noise sensitivity. Ambient temperatures were used as initial conditions for these trials. Using the average converged estimator values, the value for parameter /signal pair $\hat{\theta}_1 = 2.5$, $\hat{\theta}_2 = 0.625$. q_w is assumed to be a constant 100W.

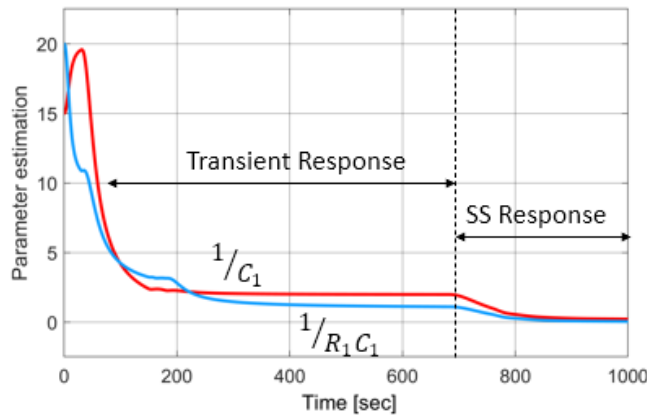


Figure 18: Estimation results for parameter R_1, C_1

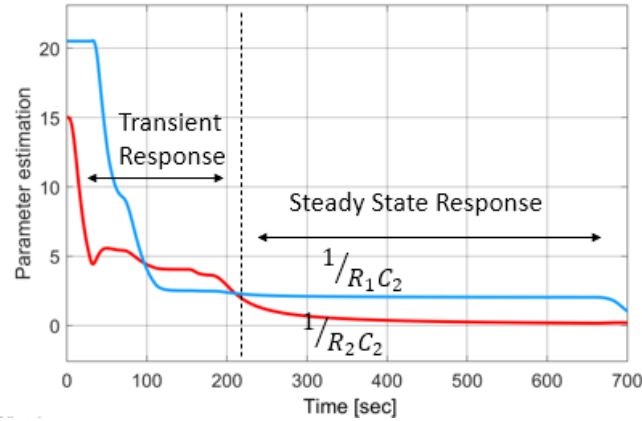


Figure 19: Estimation results for parameter R_2, C_2

Similarly thermal parameters are derived for the dynamic equation 2, and results are shown in Figure 18 and Figure 19. Transient response is due to initial variation in temperature and fuel ratio after that it is in steady state and signals converge. It concludes the thermal resistor and thermal capacitor parameter values as follows:

$$C_1 = 0.4 \text{ J/K} ; R_1 = 4 \text{ K/W} ; R_2 = 1.5 \text{ K/W} ; C_2 = 0.8 \text{ J/K}$$

These values are further used in the observer design.

3.3.2 OBSERVER DEVELOPMENT

With the estimation strategy proved effective with simulated data, the algorithm values were next used with several experimental temperature data sets obtained during clinker formation tests with the lab scale kiln. The proposed observers are to estimate the temperature at alumina tube (\hat{T}_1 Observer) and to estimate the equivalent heat source (q_w) (\hat{q}_w Observer). The resultant thermal model is utilized to design these real-time temperature observers knowing heat rate value from COMSOL and measured temperature data from test run.

For the implementation of temperature observer for a given slice, it is assumed that the measurement for $T_1(t)$ is unknown. Using thermocouple data and equation (4), a real time observer for T_1 called as $\hat{T}_1(t)$ is designed. The observer will not use the measured value for $T_1(t)$ but will use the measurements $T_2(t)$, $T_3(t)$, $T_4(t)$. For observer validation, observed temperature $\hat{T}_{AL}(t)$ is compared to the experimental data from the test run. For the lab scale kiln, it is proved for a single slice, then expanded the observer using vectors and matrices for every slice at the same time.

For slice 1,3 and 4, observer results are obtained. As shown in Figure 20, observed temperature follows the validated temperature closely for these slices. Slices 3 and 4 represent the burning zone of the kiln and as shown in the figures below. It is clear that the observed temperature closely follows the actual measured temperatures during the tests. The initial variation is due the frequent changes in fuel ratio, as it gets consistent, the observers start to track the measurement. For this trial, the kiln took approximately 5 hours to reach 1200°C. Once it reached to required temperature meal started flowing through the kiln. Figure 21. shows that during the meal, the observer is able to track the actual measured temperature. Total reside time for this test was 27 minutes. Further it was tested for remaining slices as well with satisfactory results.

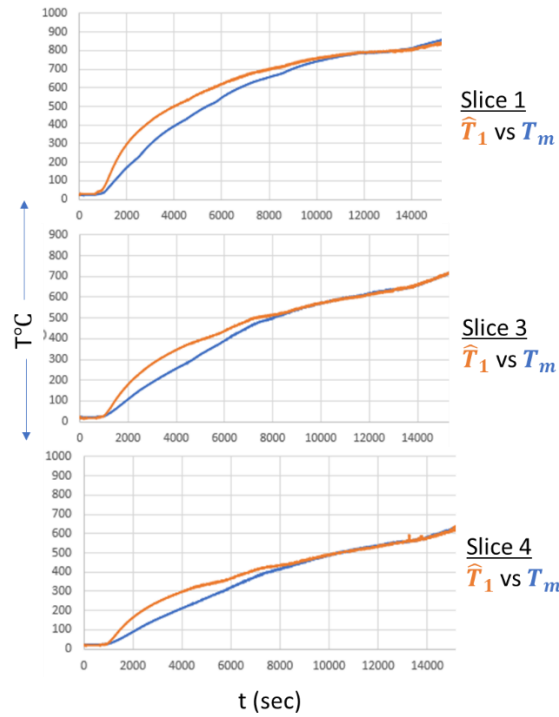


Figure 20: Observed temperature vs validated temperature of the alumina tube for slice 1 without meal

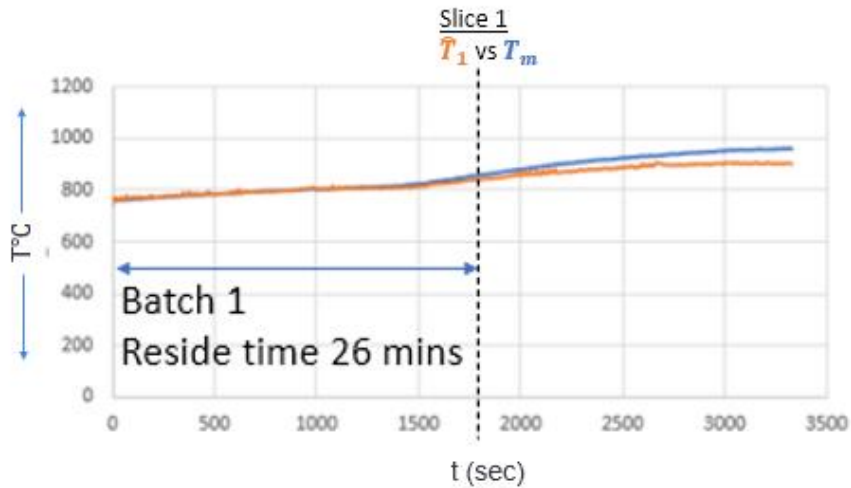


Figure 21: Observed temperature vs validated temperature of the alumina tube for slice 1 with meal

Once an estimate for $\hat{T}_1(t)$ is obtained, then using equation (3), the effective heat value of $\hat{q}_w(t)$ is observed. q_{wall} is equivalent heat source inside a given slice, shown in Figure 22. Using the combination of observers for a given slice (using equation 3 and

equation 4) the value for $q_{wall}(t)$ in real-time for every slice is observed and shown in Figure 11. The $q_{wall}(t)$ is based on reduced order model, the Multiphysics model, and the estimated parameters. As all of those are validated individually, it can be inferred that the estimation of the $q_{wall}(t)$ is accurate.

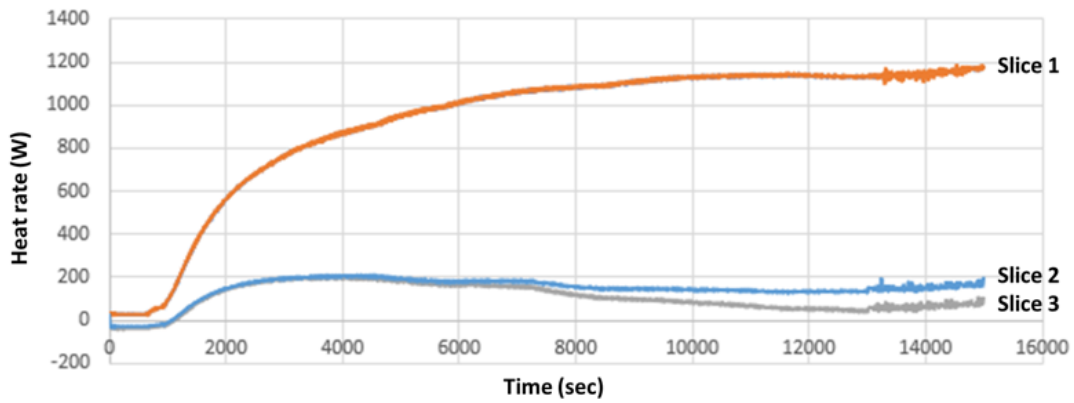


Figure 22: Heat rate observer results for three slices

4 ROTARY KILN SYSTEM MODEL

The model considered in this section is a mathematical model of the kiln, burden inside the kiln, and the electric motor[20]. This model shows the interaction of burden inside the kiln with the kiln wall. The kiln is modelled as if driven directly by only one electrical motor is shown in Figure 23 below. During startup two conditions occur namely stick and tumbling. The tumbling condition is modelled as if the burden effectively slides against the kiln wall and considered here.

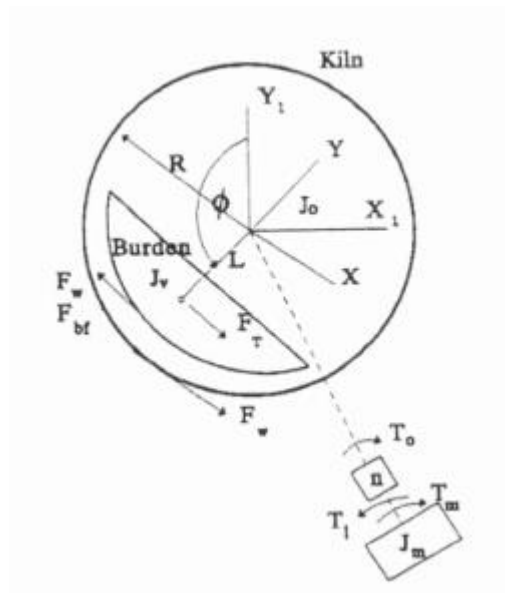


Figure 23: Kiln, burden and drive train

4.1 ROTARY KILN DYNAMIC SYSTEM MODEL

The rotational dynamics of the rotary kiln including friction torque can be modeled as

$$T_m = J_{eq}\dot{\omega}_m + \frac{1}{n}F_w R + \frac{1}{n}T \quad (48)$$

where, ω_m is the angular velocity of motor [rad/s], F_w is the friction force [N], R is the radius of the kiln [m], n is the total reduction, T is the friction torque in bearing [N.m].

Equivalent inertia for the system can be written as,

$$J_{eq} = J_m + \frac{1}{n^2}J_o \quad (49)$$

where, J_m is the inertia of the motor [kg. m^2] and J_o is the inertia of the rotary kiln [kg. m^2]. Friction torque in the bearing and the friction force can be modeled as equation (50) and (51) respectively.

$$T = 2\mu_{brg} \frac{P}{2} \cos 30^\circ \left(\frac{l+k}{2}\right) \quad (50)$$

$$F_w = \mu_c \cdot m_v \cdot g \cdot \cos (\pi + \theta_o) \quad (51)$$

where, μ_{brg} is the friction coefficient typically 0.001, l, k is the torque arm of the bearing [m], P is the total weight of the kiln [N], μ_c is the Coulomb friction coefficient, m_v is the mass of burden (material inside the kiln) [kg], g is the gravitational constant, 9.81 [m/s^2] and θ_o is the angular displacement of kiln [rad].

4.2 TORQUE OBSERVER DEVELOPMENT

A widely accept control variable in the management of the kiln burning zone placement and temperature is the rotational drive system torque, $T_{Load}(t)$. While traditional drive control systems are able to manage the kiln speed $\omega_m(t)$ without knowledge of $T_{Load}(t)$, a typical drive will provide an approximate estimator of $T_{Load}(t)$. These indicators are often approximation or even an off-line measure that has significant error as well as introducing time delay. In our work we have developed a nonlinear $\hat{T}_{Load}(t)$ observer that provide real-time load torque information that is available for the various aspect of the kiln control system. This observer can learn the trajectory of the kiln torque through minimal knowledge. Our initial observer development considers our lab-scale kiln system where we are utilizing a PMDC machine. The torque observer scheme is validated through Lyapunov-based stability analyses and PLECS simulation results are obtained which demonstrate the observer viability. This work can be update for any drive type and we will consider induction, synchronous, and hydraulic motors.

4.2.1 OBSERVER DEVELOPMENT

The main objective of the proposed observer is to track the kiln torque i.e. motor torque required to rotate the kiln such that $\hat{T}_m(t) \rightarrow T_m(t)$ as $t \rightarrow \infty$ where \hat{T}_m is the observed torque of the motor. Block diagram shown in Figure 24 represents the nonlinear observer scheme for the rotary kiln system.

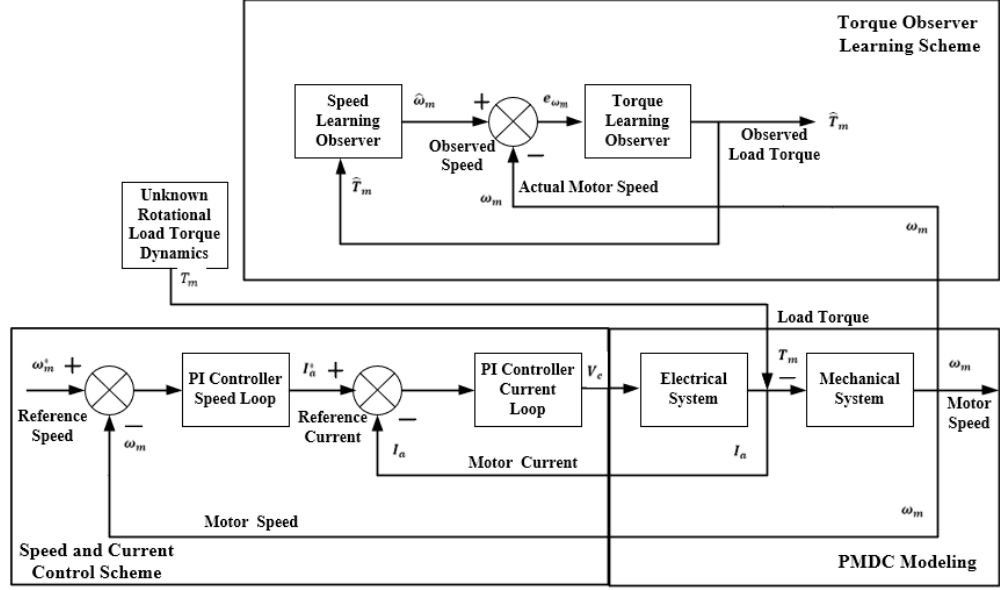


Figure 24: Schematic representation of the torque observer scheme for rotary kiln

The following assumptions are made to facilitate this observer development.

Assumption 1: The load torque $T_L(t)$ is an unknown time-varying quantity that is bounded by known function $\Omega(\omega) \geq |T_L(\omega)|$ where $\Omega(\omega)$ is continuously differentiable. It is assumed that $T_L(\omega) \in \mathcal{L}_\infty$.

Assumption 2: The signals T_m , $|\dot{T}_m|$, $|\ddot{T}_m|$ and $\dot{\omega}_m(t)$ are assumed to be piecewise continuous and bounded.

Assumption 3: The PMDC motor parameters such as R_a , L_a , k_e , k_t , B and J are known a priori and are assumed to be constant with respect to time.

Assumption 4: PMDC motor speed ω_m is measurable.

On Rearranging equation (48), it can be represented as

$$J_{eq}\dot{\omega}_m = T_m - \frac{1}{n}F_wR - \frac{1}{n}T \quad (52)$$

$$i. e. \dot{\omega}_m = \frac{1}{J_{eq}}T_m - \frac{1}{J_{eq}*n}F_wR - \frac{1}{J_{eq}*n}T. \quad (53)$$

Equation (53) in terms of torque observer and speed observer can be written as,

$$\dot{\hat{\omega}}_m = \frac{1}{J_{eq}} \hat{T}_m - \frac{1}{J_{eq} * n} F_w R - \frac{1}{J_{eq} * n} T. \quad (54)$$

Speed observer error term now can be written as,

$$e_{\omega_m} = \omega_m - \hat{\omega}_m. \quad (55)$$

such that first purpose of the observer is $e_{\omega_m} \rightarrow 0$ as $t \rightarrow \infty$. On differentiating both sides of equation (55)

$$\dot{e}_{\omega_m} = \dot{\omega}_m - \dot{\hat{\omega}}_m \quad (56)$$

Now, substituting equation (53) and equation (54) into equation (56) it can be determined as

$$\dot{e}_{\omega_m} = \frac{1}{J_{eq}} T_m - \frac{1}{J_{eq}} \hat{T}_m. \quad (57)$$

Now, filtered error signal to facilitate a closed loop system and can be defined as follows

$$S_{\omega_m} = \dot{e}_{\omega_m} + e_{\omega_m}. \quad (58)$$

Taking derivative on both sides of equation (58) it can be represented as

$$\dot{S}_{\omega_m} = \ddot{e}_{\omega_m} + \dot{e}_{\omega_m}. \quad (59)$$

Here the observer objective is $S_{\omega_m}(t) \rightarrow 0, t \rightarrow \infty$. By taking derivative of equation (57) and substituting it into equation (59) it can be seen that

$$\dot{S}_{\omega_m} = \frac{1}{J_{eq}} \dot{T}_m - \frac{1}{J_{eq}} \dot{\hat{T}}_m + \dot{e}_{\omega_m}. \quad (60)$$

From the subsequent stability analysis, the following observer is designed

$$\dot{\hat{T}}_m = J_{eq} [(k_1 + 1) * S_{\omega_m} + k_2 * \text{sgn}(e_{\omega_m})]. \quad (61)$$

Where, k_1, k_2 are positive constant gains and $sgn(\cdot)$ is the signum function. A realizable form of \hat{T}_m can be obtained by substituting (58) into (61) and integrating both sides of the resulting equation to obtain following,

$$\hat{T}_m = J_{eq} \left[\begin{array}{l} (k_1 + 1)(e_{\omega_m}(t) - e_{\omega_m}(t_0)) + \int_{t_0}^t e_{\omega_m}(\sigma) d\sigma \\ + k_2 \int_{t_0}^t sgn(e_{\omega_m}(\sigma)) d\sigma + \hat{T}_m(t_0) \end{array} \right]. \quad (62)$$

4.2.2 STABILITY ANALYSIS

Theorem 1: The torque observer in (61) ensures that $e_{\omega_m}(t), s_{\omega_m}(t) \rightarrow 0$ as $t \rightarrow \infty$.

Proof: The stability of closed loop system presented by (61) can be shown through a non-negative Lyapunov function $V_o(t) \in \mathbb{R}$ defined as

$$V_o = \frac{1}{2} e_{\omega_m}^2 + \frac{1}{2} s_{\omega_m}^2. \quad (63)$$

Taking derivative of equation (63)

$$\dot{V}_o = e_{\omega_m} \dot{e}_{\omega_m} + s_{\omega_m} \dot{s}_{\omega_m}. \quad (64)$$

On solving (58) for \dot{e}_{ω_m} and substituting it alongside (60) and simplifying yields

$$\dot{V}_o = s_{\omega_m}^2 - e_{\omega_m}^2 + \frac{s_{\omega_m}}{J_{eq}} (\dot{T}_m - \dot{\hat{T}}_m). \quad (65)$$

Substituting in (61) into (65) and rearranging eventually yield

$$\begin{aligned} \dot{V}_o = & -e_{\omega_m}^2 - k_1 s_{\omega_m}^2 + \dot{e}_{\omega_m} \frac{1}{J_{eq}} \dot{T}_m - \dot{e}_{\omega_m} k_2 sgn(e_{\omega_m}) \\ & + e_{\omega_m} \left(\frac{1}{J_{eq}} \dot{T}_m - k_2 sgn(e_{\omega_m}) \right) \end{aligned} \quad (66)$$

Integrating both sides of equation (66) gives

$$V_o = V_o(t_f) + A_1 - A_2 + A_3 - A_4 . \quad (67)$$

where,

$$A_1 = \frac{1}{J_{eq}} \int_{t_o}^t (\dot{e}_{\omega_m}(\sigma) \dot{T}_m(\sigma) d\sigma) . \quad (68)$$

$$A_2 = k_2 \operatorname{sgn}(e_{\omega_m}) \int_{t_o}^t (\dot{e}_{\omega_m}(\sigma) d\sigma) . \quad (69)$$

$$A_3 = \int_{t_o}^t e_{\omega_m}(\sigma) \left[\dot{T}_m(\sigma) - k_2 \operatorname{sgn}(e_{\omega_m}(\sigma)) \right] d\sigma . \quad (70)$$

$$A_4 = \int_{t_o}^t (e_{\omega_m}^2(\sigma) d\sigma + k_1 \int_{t_o}^t s_{\omega_m}^2(\sigma) d\sigma) . \quad (71)$$

And $V_o(t_f)$ is the final value of V_o . Using integration by parts on equation (68) yields

$$A_1 = \frac{1}{J_{eq}} (e_{\omega_m}(t) \dot{T}_m(t) - e_{\omega_m}(t_o) \dot{T}_m(t_o) - \int_{t_o}^t e_{\omega_m}(\sigma) \ddot{T}_m(\sigma) d\sigma) . \quad (72)$$

And evaluating (69) yields

$$A_2 = k_2 \operatorname{sgn}(e_{\omega_m}(t)) e_{\omega_m}(t) - k_2 \operatorname{sgn}(e_{\omega_m}(t_o)) e_{\omega_m}(t_o) . \quad (73)$$

Substituting equations (71), (72) into (67) and simplifying yields

$$V_o \leq -\frac{1}{J_{eq}} \int_{t_o}^t e_{\omega_m}^2(\sigma) d\sigma - k_1 \int_{t_o}^t s_{\omega_m}^2(\sigma) d\sigma + C . \quad (74)$$

where,

$$C = V_o(t_f) - e_{\omega_m}(t_o) \left[\frac{1}{J_{eq}} \dot{T}_m(t_o) - k_2 \operatorname{sgn}(e_{\omega_m}(t_o)) \right]$$

Since C is a constant, the derivative of (75) yields

$$V_o \leq -e_{\omega_m}^2 - k_1 s_{\omega_m}^2 . \quad (75)$$

which is negative definite all time.

Since equation (63) ≥ 0 and (75) ≤ 0 , for all time t , it can be said that $e_{\omega_m}(t), S_{\omega_m}(t) \in \mathcal{L}_\infty \cap \mathcal{L}_2$. From this it is also said that from (58) that $\dot{e}_{\omega_m} \in \mathcal{L}_\infty$. From the form of (61) it is then proved that $\dot{\hat{T}}_m \in \mathcal{L}_\infty$. Looking at (60), using *Assumption 2* it can be said that $\dot{s}_{\omega_m} \in \mathcal{L}_\infty$. Since $e_{\omega_m}, \dot{e}_{\omega_m}, s_{\omega_m}, \dot{s}_{\omega_m} \in \mathcal{L}_\infty$, then according to Barbalat's Lemma can be proved that $|e_{\omega_m}(t)|, |s_{\omega_m}(t)| \rightarrow 0$ as $t \rightarrow \infty$.

4.2.3 SIMULATION RESULTS

The parameters for the nonlinear torque observer with the rotary cement kiln are presented in **Error! Reference source not found.**. The kiln torque is considered unknown. The below figures show the simulation results for the observer. This torque observer is implemented in PLECS and simulation results are obtained.

Figure below represents the actual torque vs observed torque and actual motor speed vs observed motor speed to a step change in the desired output speed of the PMDC motor. In Figure 25 and Figure 26 it is evident that the observed value for the rotational kiln speed closely follows that of the actual value with the steady state error converge to zero.

Figure 27 presents the observed torque following the actual torque value so closely that it is visually difficult to distinguish the two lines. Figure 28 shows the error dynamics for this, which is at an extremely small magnitude. It is clear from these figures that the proposed observer works well in the closed loop control, achieving excellent torque and speed regulation.

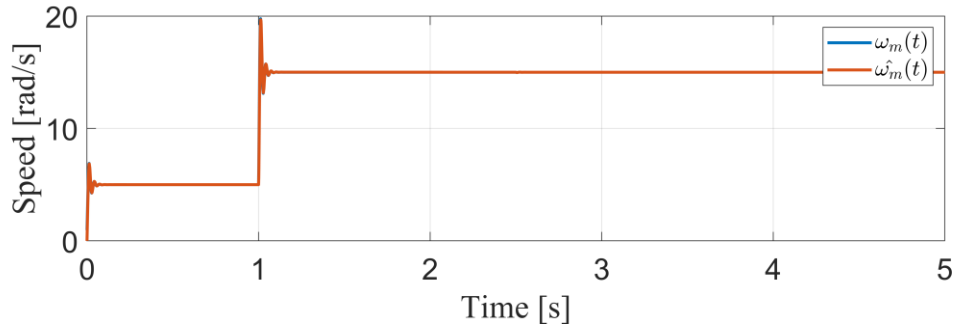


Figure 25: Actual vs observed speed for rotary kiln

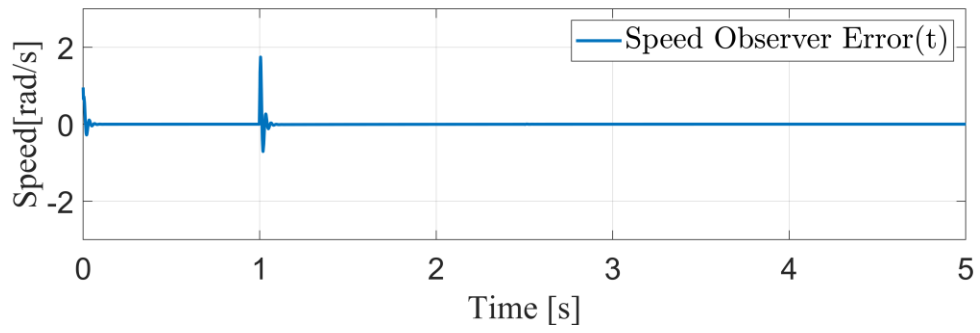


Figure 26: Speed observer error for rotary kiln

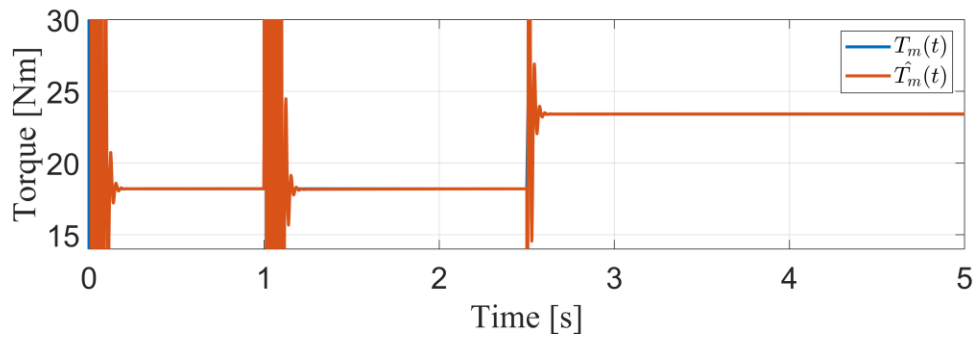


Figure 27: Actual torque vs observed torque for rotary kiln

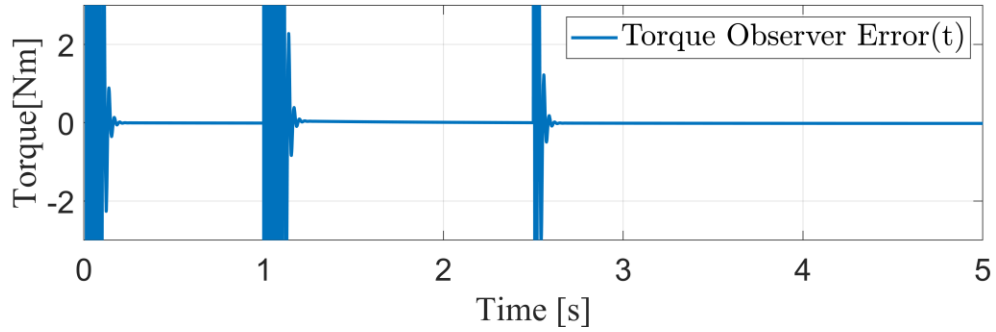


Figure 28: Torque observer error for rotary kiln

Table 1

Rotary kiln and wind torque observer parameters.

Parameter	Value	Units
k_1	1000	-
k_2	0.2	-
P	$16.512 e^6$	N
l	0.7155	m
k	0.5475	m
n	1076.5	-
R	2.17	m
J_m	0.159	$kg.m^2$
J_0	$6.978e^6$	$kg.m^2$
μ_c	0.4	-
m_v	$580e^3$	kg
J_{eq}	6.108	$kg.m^2$

4.3 TORQUE OBSERVER VALIDATION RESULTS

The primary test run of validation of the torque observer is conducted. This observer is showing the trajectory of the kiln torque through minimal knowledge. The observer development considers lab-scale kiln system where PMDC machine is utilized. The torque observer scheme is validated through Lyapunov-based stability analyses. To get motor torque, armature current is measured using LEM's current sensors in real time. More test runs are needed to get accurate measure. Figure 29 shows reference speed vs actual speed with kiln torque for a step change.

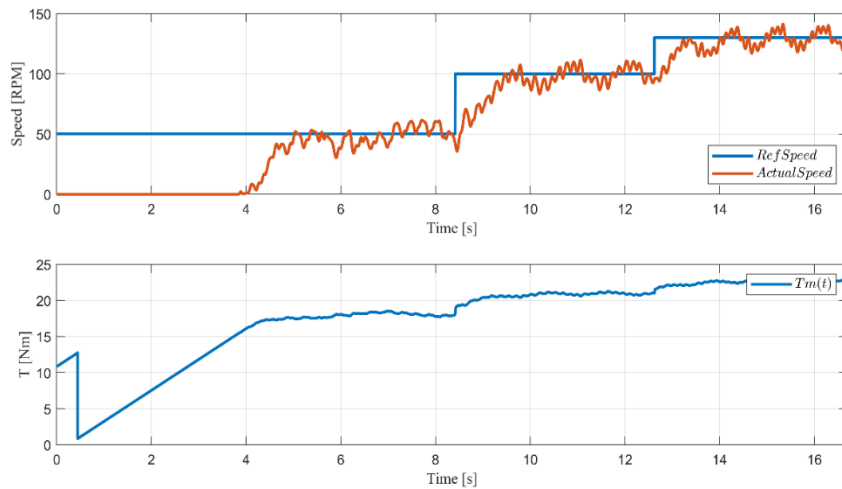


Figure 29: Validated observed kiln torque with actual motor speed vs reference speed

5 CONTROL DEVELOPMENT

5.1 PERMANENT MAGNET DIRECT CURRENT MOTOR MODEL

Operation of a rotary kiln has many challenges. In our lab-based kiln, we have a large heavy cylinder containing substantial amount of material that is rotated with a drive motor system. This means that at starting, the kiln requires high torque that can be 2.5 times the full load torque. In order to get good quality clinker, accurate control on the material flow is required so that the burner has enough time to heat the raw mix and hold it at a high temperature to ensure complete chemical reaction. Thus, accurate control of the motor speed is required. Considering all these factors, a PMDC motor was selected for its rugged construction, efficiency, accuracy, minimum maintenance cost, minimum energy use and dynamic torque regulation. Also, this motor meets the required speed and torque range, easy to control and develop observers for load torque, air flow and temperature of the kiln

5.1.1 PMDC MOTOR MODELING

To characterize the permanent magnet DC motor (PMDC), the laboratory setup shown in Figure 30 was used. This PMDC motor manufacturer did not provide the motor parameter values. Accurate mathematical models with parameters are essential for designing controllers because they are used to predict the closed loop behavior of the system. A real time controller (cRIO NI-9064) is used for speed monitoring and the data logging. With this arrangement, a variable voltage is applied to the terminals of the PMDC motor. To calculate electrical parameters of the motor, open-circuit and blocked rotor tests are conducted in the lab and the voltage vs speed characteristic is verified. To estimate armature inductance L_a and armature resistance R_a , blocked rotor test was carried out. With

the help of open circuit test, back emf constant k_e is calculated. Mechanical characteristics such as friction B and inertia J are also determined with this setup and torque speed characteristics are verified. Characterized PMDC motor parameters are listed in Table 2:

Table 2

PMSG Simulated Model Parameters

Parameter	Value	Units
J	0.1590	$\text{kg} \cdot \text{m}^2$
B	$3.9323e^{-4}$	$\text{Nm} \cdot \text{sec}/\text{rad}$
L_a	3.5	mH
R_a	1.65	Ω
k_e	3.0291	$\frac{\text{V}}{\text{rad}/\text{s}}$
k_T	3.0291	$\frac{\text{Nm}}{\text{A}}$



Figure 30: Motor control bench top testing system

5.1.2 PMDC CONTROLLER DEVELOPMENT

The cascade control structure is developed for the motor drive because of its flexibility as shown in Figure 31. It consists of distinct control loops such as innermost current loop is followed by speed loop. Motion control system often utilize a proportional-integral i.e. PI controller, hence selected. In the motion control systems, PI Controller in the speed and torque loop are often adequate hence differential i.e. D controllers are not considered here. The input to the controller is the error, which is difference between the reference input and the measured output. Cascade control requires that the bandwidth increase towards the inner loop, with the torque loop being the fastest, at crossover frequency 1kHz and the speed loop being the slowest at a crossover frequency 100Hz. Gain constants are then calculated and tested on a simulation model of PMDC Motor.

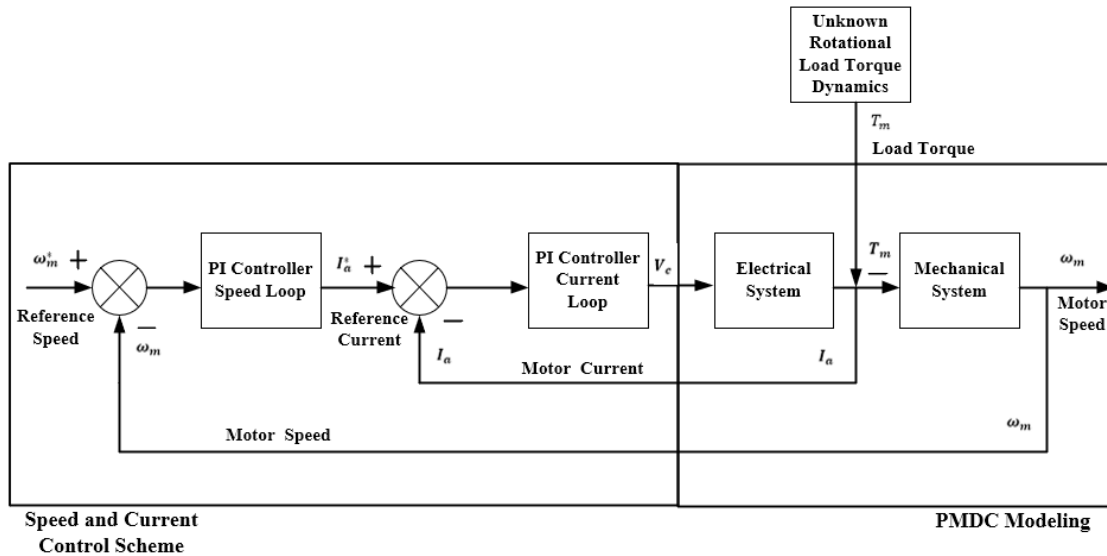


Figure 31: Block diagram of PI controller for PMDC motor with modeling

The PMDC speed control drive is also connected to the real time controller NI cRIO 9064 for automatic control application. Selected input voltage signal control coding are first developed using LabVIEW software on the personal computer and then downloaded to the onboard FPGA of the CompactRIO. NI 9381, C Series multifunction Input/Output

module have been used for this purpose. The output of the cRIO is connected to the speed control drive to adjust the motor speed. The real-time experimental results were sent back to the personal computer through real time controller of CompactRIO for monitoring and data logging. Figure 32 shows the PMDC Speed Control Drive - LabVIEW Interface.

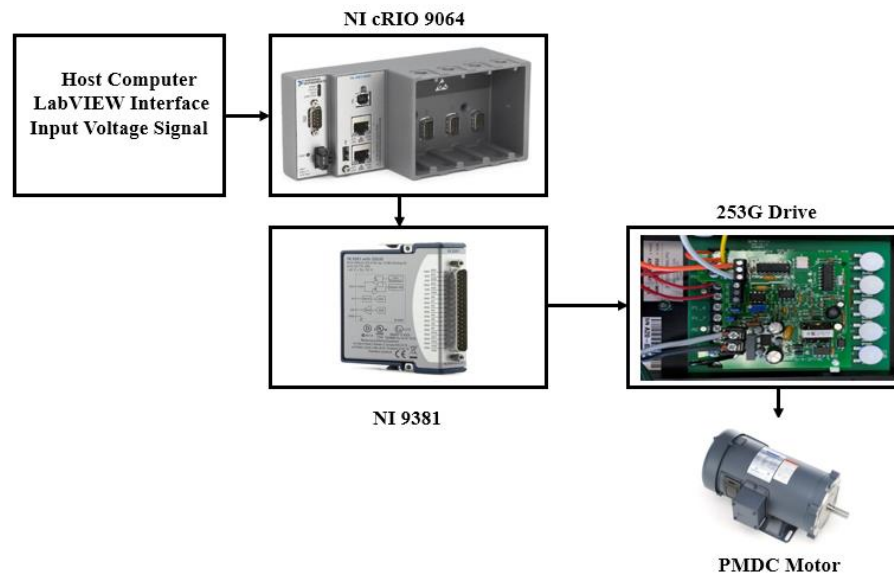


Figure 32: PMDC Speed control drive – LabVIEW interface

5.1.3 SPEED CONTROL TEST RESULTS

The below figures show the validation result for the PI controller along with controller output. The very small error shown in Figure 33 illustrate that the system is functioning well to serve the primary purpose of maintaining the desired speed through the electrical dynamics. Figure 34 shows the controller output which works well within the desired parameters in closed loop control achieving satisfactory speed regulation. For kiln-motor set up gear ratio is 112/12. Hence kiln rpm $\sim 1.8 - 2$.

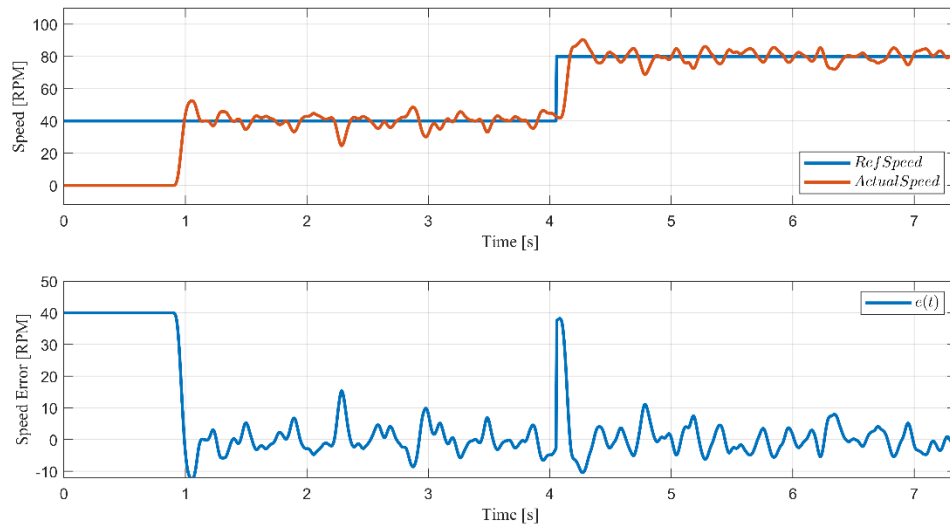


Figure 33: Reference speed vs kiln speed

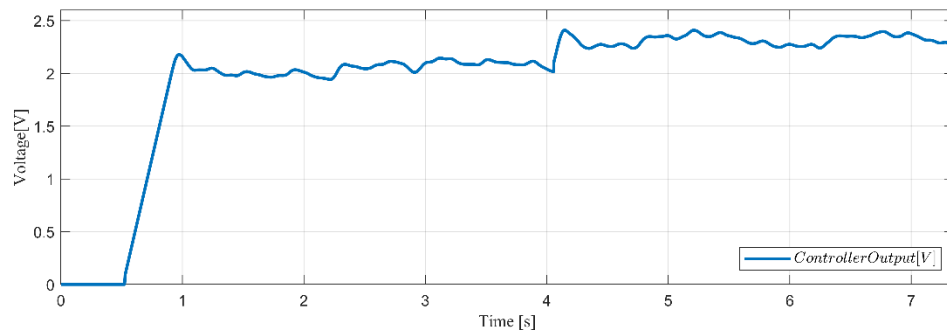


Figure 34: PI Controller output

6. FUTURE WORK

With the satisfactory results for lab scale kiln, next efforts will be taken on implementing observer for production scale kiln. For production scale kiln the approach will be different because of data availability of only inlet, outlet and skin temperature from IR cameras and pyrometers. Further in this approach is to find a lumped parameter thermal model (LPTH) that finds a good balance between the real-time data and the multi-physics model. This LPTH will be informed by the multi-Physics for material properties. Once validated various temperature sensors and energy input data will be used to develop a BZT observer. This approach will have a LPTH model for each kiln section i.e., a three-level thermal model shown below. These kiln sections will have an interconnection which captures a limited level of the thermodynamics at work within the kiln. The LPTH will be used to develop a network of observers to provide virtual temperature sensors within the kiln some limited real-time sensor data. This information can be used in both the prediction tool, and the MPC advisor to more efficiently control the kiln.

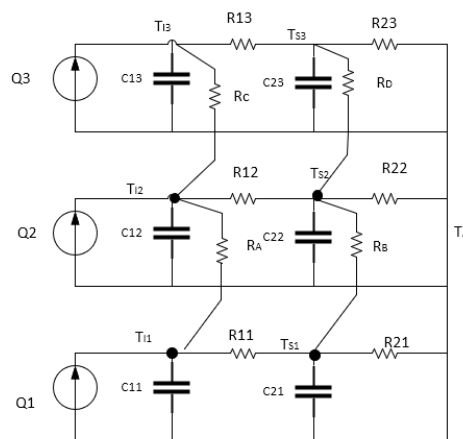


Figure 35: Three level LPTH model

From figure 35, at different temperature nodes equations can be written as

$$C_{21}\dot{T}_{s1} = -\rho T_{s1} - \rho_B T_{s2} - \rho_{21}T_A + \rho_{11}T_{I1} \quad (76)$$

$$C_{22}\dot{T}_{s2} = \rho_B T_{s1} + (-\rho_{12} - \rho_B - \rho_{22})T_{s2} + \rho_{22}T_A + \rho_{12}T_{I2} \quad (77)$$

$$C_{23}\dot{T}_{s3} = \rho_B T_{s2} + (-\rho_{13} - \rho_D - \rho_{23})T_{s3} + \rho_{23}T_A + \rho_{13}T_{I3} \quad (77)$$

where $\rho = 1/R$.

Since heat rate $Q(t)$, lumped thermal parameters such as resistance and capacitance, and skin temperature T_A , are known, $T_I(t)$ can be defined as,

$$\tilde{T}_{I1} = T_{I1} - \hat{T}_{I1} \quad (78)$$

$$\tilde{T}_{I2} = T_{I2} - \hat{T}_{I2} \quad (79)$$

$$\tilde{T}_{I3} = T_{I3} - \hat{T}_{I3} \quad (80)$$

RISE based observers' scheme will be used to design these observers and work is still in progress.

CONCLUSION

The methodology proposed in this dissertation strikes a happy medium between relying only on physical sensors and developing a full-scale analytical model. The proposed method of developing a reduced order physical based model and creation of virtual sensors based on observers has been demonstrated to work effectively on a lab scale kiln. This concept can be scaled up to apply to a real kiln with project partner Argos in future to reduce kiln energy consumption while maintaining the clinker quality.

REFERENCES

- [1] K. E. Peray and J. J. Waddell, *The rotary cement kiln*. Edward Arnold New York, 1986.
- [2] A. A. Boateng, *Rotary kilns: transport phenomena and transport processes*. Butterworth-Heinemann, 2015.
- [3] K. S. Mujumdar, A. Arora, and V. V. Ranade, "Modeling of rotary cement kilns: applications to reduction in energy consumption," *Industrial & engineering chemistry research*, vol. 45, no. 7, pp. 2315-2330, 2006.
- [4] A. Atmaca and R. Yumrutaş, "Analysis of the parameters affecting energy consumption of a rotary kiln in cement industry," *Applied Thermal Engineering*, vol. 66, no. 1-2, pp. 435-444, 2014.
- [5] P. A. Alsop, *Cement plant operations handbook: for dry process plants*. Tradeship Publications Ltd, 2007.
- [6] V. Feliu-Batlle and R. Rivas-Perez, "Design of a robust fractional order controller for burning zone temperature control in an industrial cement rotary kiln," *IFAC-PapersOnLine*, vol. 53, no. 2, pp. 3657-3662, 2020.
- [7] P. J. Juneja, S. Sunori, A. Sharma, A. Sharma, and V. Joshi, "Modeling, control and instrumentation of lime kiln process: A review," in *2020 International Conference on Advances in Computing, Communication & Materials (ICACCM)*, 2020: IEEE, pp. 399-403.
- [8] I. Bogiatzidis and A. Safacas, "Vibration analysis and backlash identification of a twin AC drive for a cement kiln," 2010.

- [9] K. Mujumdar and V. Ranade, "Simulation of rotary cement kilns using a one-dimensional model," *Chemical engineering research and design*, vol. 84, no. 3, pp. 165-177, 2006.
- [10] K. Anand, E. Mamatha, C. S. Reddy, and M. Prabha, "Design of neural network based expert system for automated lime kiln system," *Journal Européen des Systèmes Automatisés*, vol. 52, no. 4, pp. 369-376, 2019.
- [11] O. Hernandez, P. Ortiz, and J. Herrera, "Fractional PID controller with LQR proportional action applied to fractional model of cement rotary kiln," *IEEE latin America transactions*, vol. 13, no. 1, pp. 37-42, 2015.
- [12] J. Zheng, L. Zhao, and W. Du, "Hybrid model of a cement rotary kiln using an improved attention-based recurrent neural network," *ISA transactions*, 2022.
- [13] A. Wurzinger, H. Leibinger, S. Jakubek, and M. Kozek, "Data driven modeling and nonlinear model predictive control design for a rotary cement kiln," *IFAC-PapersOnLine*, vol. 52, no. 16, pp. 759-764, 2019.
- [14] R. Teja, P. Sridhar, and M. Guruprasath, "Control and optimization of a triple string rotary cement kiln using model predictive control," *IFAC-PapersOnLine*, vol. 49, no. 1, pp. 748-753, 2016.
- [15] R. N. A. Algburi, H. Gao, and Z. Al-Huda, "Design and implementation fuzzy-PLC temperature controller for the cooling tower to reduce dust emission in cement plant," in *Developments of Artificial Intelligence Technologies in Computation and Robotics: Proceedings of the 14th International FLINS Conference (FLINS 2020)*, 2020: World Scientific, pp. 1270-1279.

- [16] T. Zhongda, L. Shujiang, W. Yanhong, and W. Xiangdong, "SVM predictive control for calcination zone temperature in lime rotary kiln with improved PSO algorithm," *Transactions of the Institute of Measurement and Control*, vol. 40, no. 10, pp. 3134-3146, 2018.
- [17] M. L. McIntyre, T. J. Ghotikar, A. Vahidi, X. Song, and D. M. Dawson, "A two-stage Lyapunov-based estimator for estimation of vehicle mass and road grade," *IEEE Transactions on vehicular Technology*, vol. 58, no. 7, pp. 3177-3185, 2009.
- [18] J. Latham, M. L. McIntyre, and M. Mohebbi, "Parameter estimation and a series of nonlinear observers for the system dynamics of a linear vapor compressor," *IEEE Transactions on Industrial Electronics*, vol. 63, no. 11, pp. 6736-6744, 2016.
- [19] T. B. M McIntyre, D Dawson, B Xian, "Adaptive state of charge (SOC) estimator for a battery," presented at the 2006 American Control Conference, Minneapolis, Minnesota, USA., 2006/6/14.
- [20] a. L. P. D.J. van Dyk, "Analysis of dynamic effects in a rotary kiln system used for iron production," December 1994.

CURRICULUM VITAE

NAME: Bhagyashri Aditya Bhagwat

EDUCATION
& TRAINING:

B. E. Electrical Engineering
Shivaji University, India
2007 – 2011
Grade: 69/100

M. Eng. Electrical Engineering
Shivaji University, India
2011 – 2014
Grade: 75/100

Ph. D. Electrical and Computer Engineering
University of Louisville
2017 – 2022 (expected)
GPA: 3.80/4

PROFESSIONAL EXPERIENCE:

Graduate Research Assistant: Department of Electrical and Computer Engineering –
University of Louisville, Louisville, KY: (2019 – Present).

Graduate Teaching Assistant: Department of Electrical and Computer Engineering –
University of Louisville, Louisville, KY: (2017-2019)

Lecturer: Electrical Engineering Department – *Universal Collage of Engineering & Research, Pune, India: (2014-2015)*

Grader: University of Pune, India: (2015)

PUBLICATIONS:

Peer Reviewed Journal Papers

B. Bhagwat, M. H. Alqatamin, N. Hawkins, M. L. McIntyre, "Filter-Based Control of a Buck Converter for Uncertain Nonlinear Loads," IET Power Electronics, Vol. 13, No. 17, p 4051-4057, (2020), DOI: 10.1049/iet-pel.2020.0312.

N. Hawkins, B. Bhagwat, M. L. McIntyre, Nonlinear Current- Mode Control of SCIG Wind Turbines. *Energies* 2021, 14, 55.

Juan D. Tabares, Bhagwat B., Mark McGinley, Thad Druffel (2022), "Experimental Validation of Multiphysics Model Simulations of the Thermal Response of a Cement Clinker Rotary Kiln at Laboratory Scale", *Journal of Advanced Manufacturing and Processing*.

Peer Reviewed Conference Papers

M. H. Alqatamin, B. Bhagwat, N. Hawkins, J. Latham, M. L. McIntyre, "Self-Synchronizing Current Control for Single-Stage Three-Phase Grid-Connected Photovoltaic Systems," *2020 American Control Conference (ACC)*, Denver, CO, USA, pp. 793-797.

N. Hawkins, N. Jewell, M. H. Alqatamin, B. Bhagwat, M. L. McIntyre, "A Nonlinear Fault Detection Scheme for PV Applications," *2020 American Control Conference (ACC)*, Denver, CO, USA, pp. 3188-3192.

N. Hawkins, M. H. Alqatamin, B. Bhagwat, M. L. McIntyre, "Nonlinear Control and Observation of a PMSG Wind Turbine through Unknown Wind Torque Characteristics," *2020 American Control Conference (ACC)*, Denver, CO, USA, pp. 3188-3192.

Submitted

B. Bhagwat, M. L. McIntyre, (2022), "Parameter Estimation and Nonlinear Observers for Burning Zone Temperature Measurement with Lumped Thermal System for Rotary Cement Kiln", *Journal of Advanced Manufacturing and Processing*.

POSTER PRESENTATION:

J. Tabares, A. Ali, B. Bhagwat, M. McGinley, M. L. McIntyre, T. Druffel, (2022) Transforming the Cement Industry into Smart Manufacturing of Cement, *LAC Prize Event*, University of Louisville, KY.

TEACHING EXPERIENCE

Courses Taught

Introduction to Electrical Engineering (ECE-252) (UofL Summer 2018)

Electrical Measurements and Instrumentation (SE-EE- 203144) (UCOER 2014-2015)

Control System I (TE-EE-303147) (UCOER 2014-2015)

Power Electronics (TE-EE-303143) (UCOER 2014-2015)

Control System II (BE-EE-403145) (UCOER 2014-2015)

Power Electronic Controlled Drives (BE-EE-403148) (UCOER 2014-2015)